



1 Exploring how groundwater buffers the influence of heatwaves on 2 vegetation function during multi-year droughts

3 Mengyuan Mu¹, Martin G. De Kauwe¹, Anna M. Ukkola¹, Andy J. Pitman¹, Weidong Guo², Sanaa
4 Hobeichi¹, Peter R. Briggs³

5 ¹ARC Centre of Excellence for Climate Extremes and Climate Change Research Centre, University of New South Wales,
6 Sydney 2052, Australia

7 ²School of Atmospheric Sciences and Joint International Research Laboratory of Atmospheric and Earth System Sciences,
8 Nanjing University, Nanjing 210023, China

9 ³Climate Science Centre, CSIRO Oceans and Atmosphere, Canberra 2601, ACT, Australia

10 *Correspondence to:* Mengyuan Mu (mu.mengyuan815@gmail.com)

11 **Abstract.** The co-occurrence of droughts and heatwaves can have significant impacts on many socioeconomic and
12 environmental systems. Groundwater has the potential to moderate the impact of droughts and heatwaves by moistening the soil
13 and enabling vegetation to maintain higher evaporation, thereby cooling the canopy. We use the Community Atmosphere
14 Biosphere Land Exchange (CABLE) land surface model, coupled to a groundwater scheme, to examine how groundwater
15 influences ecosystems under conditions of co-occurring droughts and heatwaves. We focus specifically on South East Australia
16 for the period 2000–2019 when two significant droughts and multiple extreme heatwave events occurred. We found groundwater
17 plays an important role in helping vegetation maintain transpiration, particularly in the first 1–2 years of a multi-year drought.
18 Groundwater impedes gravity-driven drainage and moistens the root zone via capillary rise. These mechanisms reduced forest
19 canopy temperatures by up to 5°C during individual heatwaves, particularly where the water table depth is shallow. The role of
20 groundwater diminishes as the drought lengthens beyond 2 years and soil water reserves are depleted. Further, the lack of deep
21 roots or stomatal closure caused by high vapour pressure deficit or high temperatures can reduce the additional transpiration
22 induced by groundwater. The capacity of groundwater to moderate both water and heat stress on ecosystems during
23 simultaneous droughts and heatwaves is not represented in most global climate models, suggesting model projections may
24 overestimate the risk of these events in the future.

25 1 Introduction

26 Droughts and heatwaves are important socio-economic and environmental phenomena, impacting regional food production
27 (Kim et al., 2019; Lesk et al., 2016), water resources (Leblanc et al., 2009; Orth and Destouni, 2018) and the resilience of
28 ecosystems (Ibáñez et al., 2019; Ruehr et al., 2019; Sandi et al., 2020). When droughts and heatwaves co-occur (a “compound
29 event”) the consequences can be particularly severe, reducing the terrestrial carbon sink (Ciais et al., 2005), potentially
30 accelerating tree die-off (Allen et al., 2010, 2015; Birami et al., 2018) and setting conditions conducive for wildfires
31 (Jyoteeshkumar reddy et al., 2021). One region experiencing severe coincident heatwaves and drought is Australia (Mitchell et
32 al., 2014). Drought in Australia is associated with large-scale modes of variability, including the El Niño–Southern Oscillation
33 and the Indian Ocean Dipole (van Dijk et al., 2013), and periods of below average rainfall can extend for multiple years (Verdon-
34 Kidd and Kiem, 2009). Heatwaves are commonly synoptically driven, associated with blocking events that can be sustained
35 over many days (Perkins-Kirkpatrick et al., 2016; Perkins, 2015). Modes of variability and synoptic situations are important in
36 setting up conditions conducive to drought and heatwave. However, once a heatwave or drought has become established, land-
37 atmosphere interactions can intensify and prolong both heatwaves and droughts (Miralles et al., 2019), affect their intensity and
38 influence the risk of their co-occurrence (Mukherjee et al., 2020). The role of the land surface in amplifying or dampening
39 heatwaves and droughts is associated with the partitioning of available energy between sensible and latent heat (Fischer et al.,
40 2007; Hirsch et al., 2019) and is regulated by sub-surface water availability (Teuling et al., 2013; Zhou et al., 2019). As soil



41 moisture becomes more limiting, more of the available energy is converted into sensible heat, reducing evaporative cooling via
42 latent heat. Changes in the surface turbulent energy fluxes influence the humidity in the boundary layer, the formation of clouds,
43 incoming solar radiation and the generation of rainfall (D’Odorico and Porporato, 2004; Seneviratne et al., 2010; Zhou et al.,
44 2019). The sensible heat fluxes warm the boundary layer, leading to heat that can accumulate over several days and exacerbate
45 heat extremes (Miralles et al., 2014), which can in turn increase the atmospheric demand for water and intensify drought
46 (Miralles et al., 2019; Schumacher et al., 2019).

47

48 Vegetation access to groundwater has the potential to alter these land-atmosphere feedbacks by maintaining vegetation function
49 during extended dry periods, supporting transpiration and moderating the impact of droughts and heatwaves (Marchionni et al.,
50 2020; Miller et al., 2010). Where the water table is relatively shallow, capillarity may bring water from the groundwater towards
51 the surface root zone, increasing plant water availability. Where the water table is deeper, phreatophytic vegetation with tap
52 roots can directly access groundwater (Zencich et al., 2002). The presence of groundwater, and the access to groundwater by
53 vegetation is therefore likely to buffer vegetation drought and heatwave stress. For example, groundwater may help vegetation
54 sustain transpiration and consequently cool plant canopies via evaporation. This is particularly critical during compound events
55 where cessation of transpiration would increase the risk of impaired physiological function and the likelihood that plants would
56 exceed thermal limits and risk mortality (Geange et al., 2021; O’sullivan et al., 2017; Sandi et al., 2020).

57

58 Quantifying the influence of groundwater on vegetation function has remained challenging as concurrent observations of
59 groundwater dynamics, soil moisture, and energy and water fluxes are generally lacking over most of Australia and indeed
60 many parts of the world. Land surface models (LSMs) provide an alternative tool for studying the interactions between
61 groundwater, vegetation, and surface fluxes in the context of heatwaves and droughts (Gilbert et al., 2017; Martinez et al., 2016a;
62 Maxwell et al., 2011; Shrestha et al., 2014). However, there has been very little work focused on the influence of groundwater
63 on droughts and heatwaves occurring at the same time (Keune et al., 2016; Zipper et al., 2019). Our key goal in this paper is
64 therefore to examine the timescales and extent to which vegetation utilises groundwater during drought and heatwaves, and
65 determine the degree to which groundwater can mitigate the impacts of compound extremes. We focus on droughts and
66 heatwaves occurring over south-eastern (S.E.) Australia between during 2000–2019 using the Community Atmosphere
67 Biosphere Land Exchange (CABLE) LSM. S.E. Australia is an ideal case study since its forest and woodland ecosystems are
68 known to be dependent on groundwater (Eamus and Froend, 2006; Kuginis et al., 2016; Zencich et al., 2002) and it has
69 experienced two multi-year droughts and record-breaking heatwaves over the last two decades. By examining the role of
70 groundwater in influencing droughts and heatwaves, and by understanding how well CABLE can capture the relevant processes,
71 we aim to build confidence in the simulations of land-atmosphere interactions for future droughts and heatwaves.

72 **2 Methods**

73 **2.1 Study area**

74 The climate over S.E. Australia varies from humid temperate near the coast to semi-arid in the interior. In the last 20 years, S.E.
75 Australia experienced the 9-year Millennium drought during 2001–2009 (van Dijk et al., 2013) where rainfall dropped from a
76 climatological average (1970–1999) of 542 mm yr⁻¹ to 449 mm yr⁻¹, and a 3-year intense recent drought during 2017–2019
77 where rainfall dropped to 354 mm yr⁻¹ (Figure S1). It has also suffered record-breaking summer heatwaves in 2009, 2013, 2017,
78 and 2019 (Bureau of Meteorology, 2013, 2017, 2019; National Climate Centre, 2009). Here we investigate groundwater
79 interactions during the period 2000–2019, focusing on the Millennium drought (MD, 2001–2009) and the recent drought (RD,
80 2017–2019).



81 2.2 Overview of CABLE

82 CABLE is a process-based LSM that simulates the interactions between climate, plant physiology and hydrology (Wang et al.,
83 2011). Above ground, CABLE simulates the exchange of carbon, energy and water fluxes, using a single layer, two-leaf
84 (sunlit/shaded) canopy model (Wang and Leuning, 1998), with a treatment of within-canopy turbulence (Raupach, 1994;
85 Raupach et al., 1997). CABLE includes a 6-layer soil model (down to 4.6 m) with soil hydraulic and thermal characteristics
86 dependent on the soil type and soil moisture content. CABLE has been extensively evaluated (e.g., Abramowitz et al., 2008;
87 Wang et al., 2011; Zhang et al., 2013) and benchmarked (Abramowitz 2012; Best et al. 2015) at global and regional scales.
88 Here we adopt a version of CABLE (Decker, 2015; Decker et al., 2017) which includes a dynamic groundwater component
89 with aquifer water storage. This version, CABLE-GW, has been previously evaluated by Decker (2015), Ukkola et al. (2016b)
90 and Mu et al. (2021) and shown to perform well for simulating water fluxes. CABLE code is freely available upon registration
91 (<https://trac.nci.org.au/trac/cable/wiki>); here we use CABLE SVN revision 7765.

92 2.3 Hydrology in CABLE-GW

93 The hydrology scheme in CABLE-GW solves the vertical redistribution of soil water via a modified Richards equation (Zeng
94 and Decker, 2009):

$$96 \frac{\partial \theta}{\partial t} = -\frac{\partial}{\partial z} K \frac{\partial}{\partial z} (\Psi - \Psi_E) - F_{soil} \quad (1)$$

97
98 where θ is the volumetric water content of the soil ($\text{mm}^3 \text{mm}^{-3}$), K is the hydraulic conductivity (mm s^{-1}), z is the soil depth
99 (mm), Ψ and Ψ_E are the soil matric potential (mm) and the equilibrium soil matric potential (mm), and F_{soil} is the sum of
100 subsurface runoff and transpiration (mm s^{-1}) (Decker, 2015). To simulate groundwater dynamics, an unconfined aquifer is added
101 to the bottom of the soil column with a simple water balance model:

$$103 \frac{dW_{aq}}{dt} = q_{re} - q_{aq,sub} \quad (2)$$

104
105 where W_{aq} is the mass of water in the aquifer (mm), $q_{aq,sub}$ is the subsurface runoff in the aquifer (mm s^{-1}), and q_{re} is the water
106 flux between the aquifer and the bottom soil layer (mm s^{-1}) computed by the modified Darcy's law:

$$108 q_{re} = K_{aq} \frac{(\Psi_{aq} - \Psi_n) - (\Psi_{E,aq} - \Psi_{E,n})}{z_{wtd} - z_n} \quad (3)$$

109
110 where K_{aq} is the hydraulic conductivity within the aquifer (mm s^{-1}), Ψ_{aq} and $\Psi_{E,aq}$ are the soil matric potentials for the aquifer
111 (mm), and Ψ_n and $\Psi_{E,n}$ are the soil matric potentials for the bottom soil layer (mm). z_{wtd} and z_n are the depth of the water table
112 (mm) and the lowest soil layer (mm), respectively. CABLE-GW assumes the groundwater aquifer sits above impermeable
113 bedrock, giving a bottom boundary condition of:

$$115 q_{out} = 0 \quad (4)$$

116
117 CABLE-GW computes the subsurface runoff (q_{sub} , mm s^{-1}) using:

$$119 q_{sub} = \sin \frac{dz}{di} \hat{q}_{sub} e^{-\frac{z_{wtd}}{fp}} \quad (5)$$



120

121 where $\overline{\frac{dz}{dt}}$ is the mean subgrid-scale slope, \hat{q}_{sub} is the maximum rate of subsurface drainage (mm s^{-1}) and f_p is a tunable
122 parameter. q_{sub} is generated from the aquifer and the saturated deep soil layers (below the third soil layer).

123 2.4 Experiment design

124 To explore how groundwater influences droughts and heatwaves, we designed two experiments, with and without groundwater
125 dynamics, driven by the same 3-hour meteorology forcing and land surface properties (see section 2.5 for datasets) for the period
126 1970-2019. To correct a tendency for high soil evaporation, we implemented a parameterisation of soil evaporation resistance
127 that has previously been shown to improve the model (Decker et al., 2017; Mu et al., 2021).

128 2.4.1 Groundwater experiment (GW)

129 This simulation uses the default CABLE-GW model, which includes the unconfined aquifer to hold the groundwater storage
130 and simulates the water flux between the bottom soil layer and the aquifer. We first ran the default CABLE-GW with fixed CO_2
131 concentrations at 1969 levels for 90 years by looping the meteorology forcing over 1970–1999. At the end of the 90-year spin-
132 up, moisture in both the soil column and the groundwater aquifer reached an effective equilibrium when averaged over the study
133 area. We then ran the model from 1970 to 2019 with time varying CO_2 . We omit the first 30 years of this period and analyse
134 the period 2000–2019 to allow for further equilibrium with the time-evolving CO_2 .

135 2.4.2 Free drainage experiment (FD)

136 Many LSMs, including those used in the Coupled Model Intercomparison Project 5 (CMIP5), still use a free drainage
137 assumption and neglect the parameterisation of the unconfined aquifer. To test the impact of this assumption we decoupled the
138 aquifer from the bottom soil layer and thus removed the influence of groundwater dynamics (experiment FD). In FD, at the
139 interface between the bottom soil layer and the aquifer, soil water can only move downwards as vertical drainage at the rate
140 defined by the aquifer hydraulic conductivity:

141

$$142 \quad q_{re} = K_{aq} \quad (6)$$

143

144 This vertical drainage is added to the subsurface runoff flux:

145

$$146 \quad q_{sub} = q_{sub} + q_{re} \quad (7)$$

147

148 The simulated water table depth (WTD) in CABLE-GW affects the water potential gradient between the soil layers via Ψ_E
149 (Zeng and Decker, 2009) and impacts q_{sub} (Equation 5). However, in FD, decoupling the soil column from the aquifer and
150 adding vertical drainage directly to subsurface runoff causes an artificial and unrealistic decline in WTD. To solve this problem,
151 we assume a fixed WTD in the FD simulations at 10 m in order to remove this artefact from the simulation of Ψ_E and q_{sub} .

152 The FD simulations are initialized from the near-equilibrated state at the end of the 90-year spin-up used in GW. The period
153 1970–2019 is then simulated using varying CO_2 and the last 20 years are used for analysis.

154 2.4.3 Deep root experiment (DR)

155 The parameterisation of roots, including the prescription of root parameters in LSMs, is very uncertain (Arora and Boer, 2003;
156 Drewniak, 2019) and LSMs commonly employ root distributions that are too shallow (Wang and Dickinson, 2012). The vertical
157 distribution of roots influences the degree to which plants can utilise groundwater, and potentially the role groundwater plays



158 in influencing droughts and heatwaves. To explore the uncertainty associated with root distribution, we added a “deep root”
159 (DR) experiment by increasing the effective rooting depth in CABLE for tree areas. In common with many LSMs, CABLE-
160 GW defines the root distribution following Gale and Grigal (1987):

161

$$162 \quad f_{root} = 1 - \beta_{root}^z \quad (8)$$

163

164 where f_{root} is the cumulative root fraction (between 0 and 1) from the soil surface to depth z (m), and β_{root} is a fitted parameter
165 specified for each plant functional type (PFT) (Jackson et al., 1996). In CABLE, the tree areas in our study region are simulated
166 as evergreen broadleaf PFT with a $\beta_{root} = 0.962$, implying that only 8% of the simulated roots are located below a depth of 64
167 cm. However, field observations (Canadell et al., 1996; Eberbach and Burrows, 2006; Fan et al., 2017; Griffith et al., 2008)
168 suggest that the local trees tend to have a far deeper root system, possibly to help cope with the high climate variability. We
169 therefore increased β_{root} for the evergreen broadleaf PFT to 0.99, which assumes 56% of roots are located in depths below
170 64cm and 21 % of roots below 1.7 m. This enables the roots to extract larger quantities of deep soil water moisture, which is
171 more strongly influenced by groundwater.

172

173 This is a simple sensitivity study, and we therefore only run this experiment during January 2019, when record-breaking
174 heatwaves compound with the severe recent drought. The DR experiment uses identical meteorology forcing and land surface
175 properties as GW and FD, and is initialised by the state of the land surface on the 31st December 2018 from the GW experiment.

176 2.5 Datasets

177 Our simulations are driven by the atmospheric forcing from the Australian Water Availability Project (AWAP), which provides
178 daily gridded data covering Australia at 0.05° spatial resolution (Jones et al., 2009). This dataset has been widely used to force
179 LSMs for analysing the water and carbon balances in Australia (Haverd et al., 2013; De Kauwe et al., 2020; Raupach et al.,
180 2013; Trudinger et al., 2016). The AWAP forcing data include observed fields of precipitation, solar radiation, minimum and
181 maximum daily temperatures and vapour pressure at 9 am and 3 pm. Since AWAP forcing does not include wind and air pressure
182 we adopted the near-surface wind speed data from McVicar et al. (2008) and assume a fixed air pressure of 1000 hPa. Due to
183 missing observations before 1990, the solar radiation input for 1970–1989 was built from the 1990–1999 daily climatology.
184 Similarly, wind speeds for 1970–1974 are built from the 30-year climatology from 1975 to 2004. We translated the daily data
185 into 3-hourly resolution using a weather generator (Haverd et al., 2013).

186

187 The land surface properties for our simulations are prescribed based on observational datasets. Land cover type is derived from
188 the National Dynamic Land Cover Data of Australia (DLCD) (<https://www.ga.gov.au/scientific-topics/earth-obs/accessing-satellite-imagery/landcover>). We classify DLCD’s land cover types to five CABLE PFTs: crop (irrigated/rainfed crop, pasture
189 and sugar DLCD classes), broadleaf evergreen forest (closed/open/scattered/sparse tree), shrub (closed/open/scattered/sparse
190 shrubs and open/scattered/sparse chenopod shrubs), grassland (open/sparse herbaceous) and barren land (bare areas). The leaf
191 area index (LAI) in CABLE is prescribed using a monthly climatology derived from the Copernicus Global Land Service
192 product (<https://land.copernicus.eu/global/products/lai>). The climatology was constructed by first creating a monthly time series
193 by taking the maximum of the 10-daily timesteps each month and then calculating a climatology from the monthly data over
194 the period 1999–2017. The LAI data was resampled from the original 1 km resolution to the 0.05° resolution following De
195 Kauwe et al. (2020). Soil parameters are derived from the soil texture information (sand/clay/silt fraction) from SoilGrids (Hengl
196 et al., 2017) via the pedotransfer functions in Cosby et al. (1984) and resampled from 250 m to 0.05° resolution.

198



199 To evaluate the model simulations, we use monthly total water storage anomaly (TWSA) at 0.5° spatial resolution from the
200 Gravity Recovery and Climate Experiment (GRACE) and GRACE Follow On products (Landerer et al., 2020; Watkins et al.,
201 2015; Wiese et al., 2016, 2018). The RLM06M release is used for February 2002 – June 2017 and for June 2018 – December
202 2019. We also use the total land evaporation from the Global Land Evaporation Amsterdam Model (GLEAM version 3.5,
203 https://www.gleam.eu/; Martens et al., 2017; Miralles et al., 2011) at 0.5° spatial resolution. For daytime land surface
204 temperature (LST) we use the Moderate Resolution Imaging Spectroradiometer (MODIS) datasets from Terra and Aqua
205 satellites (products MOD11A1 and MYD11A1, Wan and Li, 1997; Wan 2015a, 2015b) at 1 km spatial resolution. We only
206 consider pixels and time steps identified as good quality (QC flags 0). Only the day-time LST values are used due to the lack of
207 good quality night-time LST data. The Terra overpass occurs at 10 am and Aqua at 2 pm local time. To analyse the compound
208 events in January 2019, we linearly interpolate the 3-hourly model outputs to 2 pm to match the overpass time of the Aqua LST.
209 The GRACE, GLEAM and MODIS datasets were resampled to the AWAP resolution using bilinear interpolation.

210

211 To evaluate model performance during heatwaves, we identify heatwave events using the excess heat factor index (EHF, Nairn
212 and Fawcett, 2014). EHF is calculated using the daily AWAP maximum temperature, as the product of the difference of the
213 previous 3 day mean to the 90th percentile of the 1970–1999 climatology and the difference of the previous 3 day mean to the
214 preceding 30 day mean. A heatwave occurs when the EHF index is greater than 0 for at least three consecutive days. We only
215 focus on summer heatwaves occurring between December and February of the following year.

216

217 **3 Results**

218 **3.1 Simulations for the Millennium Drought and the recent drought**

219 Previous studies have shown that simulations by LSMs diverge as the soil dries (Ukkola et al., 2016a), associated with
220 systematic biases in evaporative fluxes and soil moisture states in the models (Mu et al., 2021; Swenson and Lawrence, 2014;
221 Trugman et al., 2018). We therefore first evaluate how well CABLE-GW captures the evolution of terrestrial water variability
222 during two recent major droughts.

223

224 Figure 1a shows the total water storage anomaly during 2000–2019 observed by GRACE and simulated in GW and FD. Both
225 GW and FD accurately capture the interannual variability in total water storage for S.E. Australia ($r = 0.96$ in GW, and 0.90 in
226 FD). Both model configurations simulate a decline in TWSA through the first drought period (up to 2009, see Figure S1), the
227 rapid increase in TWSA from 2010 associated with higher rainfall, a decline from around 2012 due to the re-emergence of
228 drought conditions, and the rapid decline during the recent drought after conditions had eased in 2016 (Figure S1). FD
229 underestimates the magnitude of monthly TWSA variance (standard deviation, $SD = 37.18$ mm) compared to GRACE (47.74
230 mm) or GW (47.67 mm). This underestimation is linked with the lack of aquifer water storage in the FD simulations which
231 provides a reservoir of water that changes slowly and has a memory of previous wet/dry climate conditions (Figure 1a).

232

233 Figure 1b shows the accumulated precipitation (P) minus evaporation (E) over the two drought periods. GW increases the
234 evaporation relative to FD such that the accumulated P–E decreases from about 786 mm to 455 mm during the Millennium
235 drought, which is much closer to the GLEAM estimate (97 mm). A similar result, although over a much shorter period, is also
236 apparent for the recent drought (Figure 1b). The lower P–E in GW suggests that the presence of groundwater storage alleviates
237 the vegetation water stress during droughts, and reduces the reliance of E on P, indicated by a small reduction in the correlation
238 (r) between E and P from 0.28 in FD to 0.24 in GW for MD, and a reduction from 0.42 to 0.37 for RD (Figure 1b). The GW
239 simulations are also closer to the GLEAM estimates which suggests that adding groundwater improves the simulations during



240 droughts. The difference in E is also demonstrated spatially in Figure S2. During the Millennium drought, the GW simulations
241 show a clear improvement over FD in two aspects. GW shows smaller biases in E along the coast where FD underestimates E
242 strongly (Figure S2b-c). The areas where E is underestimated are also smaller in extent in GW, suggesting that GW overall
243 reduces the dry bias. The magnitude of the bias in GW reaches around 300 mm over small areas of S.E. Australia while in the
244 FD simulations biases are larger, reaching 400 mm over a larger area. Overall, Figure 1 and Figure S2 show that representing
245 groundwater improves the simulation of the inter-annual variability in the terrestrial water cycle and storage, particularly during
246 droughts.

247 3.2 The role of groundwater in sustaining evaporation during droughts

248 We next explore the mechanisms by which including groundwater modifies the simulation of evaporation. Figure 2 displays the
249 overall influence of groundwater on water fluxes during the recent drought. GW simulates 50–200 mm yr⁻¹ more E over coastal
250 regions where there is high tree cover (Figure 2a; see Figure S3 for land cover). Adding groundwater also increases E in most
251 other regions, although the impact is negligible in many inland and non-forested regions (i.e., west of 145°E). We identified a
252 clear connection between E (Figure 2a) and the simulated WTD in the GW simulations (Figure S4). GW simulates 110 mm yr⁻¹
253 more E when the WTD is shallower than 5 m deep, 22 mm yr⁻¹ when the WTD is 5–10 m deep, but only 3 mm yr⁻¹ more when
254 the WTD is below 10 m. Higher transpiration (ΔE_t) in GW explains 78% of the total evaporative difference between GW and
255 FD where WTD is shallower than 5 m (Figure 2b). This is confirmed by the change in the soil evaporation (ΔE_s) (Figure 2c)
256 where adding groundwater increases E_s by negligible amounts over most of S.E. Australia, but by up to 25 mm yr⁻¹ in regions
257 underlain by shallow groundwater (Figure S4), which is consistent with field observations that indicate that E_s can be substantial
258 under conditions of a very shallow water table (Thorburn et al., 1992). In the very shallow WTD areas, the excess E_s in GW
259 results from the capillary rise of moisture from the shallow groundwater to the surface.

260
261 A significant factor in explaining how groundwater influences E is through changes in drainage and recharge from the aquifer.
262 Figure 2d shows that the vertical drainage (D_r) both increases and decreases depending on the location. The addition of
263 groundwater reduces vertical drainage by 74 mm yr⁻¹ where WTD is shallower than 5 m. In some regions, the drainage increases
264 with the inclusion of groundwater by up to 100 mm yr⁻¹, especially in the areas where WTD is ~ 5 m. This is associated with
265 the WTD being slightly below the bottom of the soil column (4.6 m). When the groundwater aquifer is nearly full and the bottom
266 soil layer is relatively wet, the calculated hydraulic conductivity (K_{aq}) in GW is much larger than in FD where the bottom soil
267 layer is drier due to a lack of groundwater contribution. This leads to higher vertical drainage in GW and a positive ΔD_r . Inland,
268 where the WTD tends to be much deeper there is no significant difference in D_r between GW and FD.

269
270 Figure 2e shows the difference in recharge into the upper soil column (ΔQ_{rec}) between GW and FD. The recharge from the
271 aquifer into the bottom soil layer provides 17 mm yr⁻¹ extra moisture in the GW simulations in regions with a WTD between
272 5–10 m and 10 mm yr⁻¹ where the WTD is deeper than 10 m, helping to explain the changes in E and E_t in areas with deep
273 WTD. However, there is no significant ΔQ_{rec} in regions with a shallow WTD (~5 mm yr⁻¹), suggesting the influence of
274 groundwater is mainly via reduced drainage in these locations. Recharge can only occur when WTD is below the soil column
275 (bottom boundary at 4.6m depth). If WTD is shallow and within the soil column, the interface is saturated and no recharge from
276 the aquifer to the soil column can occur and water only moves downwards by gravity.

277
278 The combined impact of reduced drainage in GW (Figure 2d) and recharge into the root-zone (Figure 2e) is an increased water
279 potential gradient between the drier top soil layers and the wetter deep soil layers, encouraging overnight capillary rise. Taking
280 the hot and dry January 2019 as an example, when the compound events occurred, Figure 2f shows the maximum water stress
281 factor difference ($\Delta\beta$) overnight (between 9 pm and 3 am, i.e. predawn when soil is relatively moist following capillary lift



282 overnight). We only consider rainless nights to exclude the impact of drainage induced by precipitation. The water stress factor
283 (β) is based on the root distribution and moisture availability in each soil layer and represents the soil water stress on transpiration
284 as water becomes limiting. Figure 2f implies that while the redistribution of moisture is small overall, in some locations it can
285 reduce moisture stress by up to 4–6%.

286 3.3 The impact of groundwater during heatwaves

287 We next explore whether the higher available moisture due to the inclusion of groundwater enables the canopy to cool itself via
288 evaporation during heatwaves by examining the temperature difference between the simulated canopy temperature (T_{canopy} , °C)
289 and the forced air temperature (T_{air} , °C). We focus on the forested regions (Figure S3) as the role of groundwater in enhancing
290 plant water availability was shown to be largest in these regions (Figure 2).

291

292 Figure 3a shows the average $T_{\text{canopy}} - T_{\text{air}}$ (ΔT , °C) over the forested regions for summer heatwaves from the GW and FD
293 simulations, with the grey line indicating the median ΔT difference. During heatwaves, the inclusion of groundwater moistens
294 the soil and supports higher transpiration, cooling the canopy and reducing ΔT relative to FD by up to 0.76°C (e.g. January
295 2013). As the drought lengthens in time (Figure 1a), the depletion of moisture gradually reduces this effect. The impact of
296 groundwater is clear in the evaporative fraction (Figure 3b) where in periods of higher rainfall (e.g. 2010–2011; Figure S1), and
297 at the beginning of a drought (2001, 2017), the EF is higher (0.03 to 0.18). This implies more of the available energy is
298 exchanged with the atmosphere in the form of latent, rather than sensible heat. However, the strength of the cooling effect
299 decreases as the droughts extends, because the vegetation becomes increasingly water-stressed which consequently limits
300 transpiration (Figure 3c).

301

302 Figure 4a shows the spatial map of ΔT simulated in GW during heatwaves in the 2017–2019 drought. It indicates both land
303 cover type (Figure S3) and WTD (Figure S4) contribute to the ΔT pattern. The evaporative cooling via transpiration is stronger
304 over the forested areas compared to crop or grassland, and stronger in the regions with a wetter soil associated with a shallower
305 WTD. However, EF is mainly determined by WTD (compare Figure 4b and Figure S4). Inland, where the WTD is deeper and
306 the soil is drier, most of the net radiation absorbed by the land surface is partitioned into sensible rather than latent heat (Figure
307 4b). However, in the coastal regions with a shallow WTD, the wetter soil reduces the water stress (Figure 4c), enables a higher
308 EF (Figure 4b), and alleviates heat stress on the leaves (Figure 4a). Along the coast where WTD is shallow, GW simulates a
309 cooler canopy temperature due to the higher evaporative cooling (Figure 4e) which is the consequence of a lower soil water
310 stress (Figure 4f) linked to the influence of groundwater (Figure S4).

311

312 Figure 5 shows the density scatter plot of ΔT versus WTD in S.E. Australia forested areas during heatwaves in 2000–2019. A
313 shallow WTD moderates the temperature difference between the canopy and the ambient air during heatwaves leading to a
314 smaller temperature difference. Meanwhile, as the WTD increases, due to the limited rooting depth in the model, the ability of
315 the groundwater to support transpiration and offset the impact of high air temperatures is reduced. Figure 5 shows a large amount
316 of variations, but nonetheless implies a threshold of ~6 m whereafter there is a decoupling and little influence from groundwater
317 during heatwaves.

318 3.4 The impact of groundwater during the drought and heatwave compound events

319 To examine the influence of groundwater on heatwaves occurring simultaneously with drought, we focus on a case study of the
320 record-breaking heatwaves in January 2019, which is the hottest month on record for the study region (Bureau of Meteorology,
321 2019). The unprecedented prolonged heatwave period started in early December 2018 and continued through January 2019 with
322 three peaks. We select two days (15th and 25th January 2019), when heatwaves spread across the study region, from the second



323 and third heatwave phases (Figure S5).

324

325 We evaluate CABLE T_{canopy} against MODIS LST observations, concentrating on forested areas where MODIS LST should
326 more closely reflect vegetation canopy temperatures, but note that this comparison is not direct as the satellite estimate will
327 contain contributions from the understorey and soil. Figures 6a-b show the good quality MODIS LST minus T_{air} at 2 pm
328 ($\Delta T_{\text{MOD}_2\text{pm}}$) over forested regions on the 15th and 25th January 2019, and Figures 6c-d display the matching GW-simulated ΔT
329 at 2 pm ($\Delta T_{\text{GW}_2\text{pm}}$). Overall, $\Delta T_{\text{GW}_2\text{pm}}$ increases from the coast to the interior in both heatwaves, consistent with the $\Delta T_{\text{MOD}_2\text{pm}}$
330 pattern in both heatwaves, albeit that $\Delta T_{\text{GW}_2\text{pm}}$ appears to be biased high relative to $\Delta T_{\text{MOD}_2\text{pm}}$ along the coastal forests (Figure
331 S6a-b).

332

333 Figure 6e-f shows the $\Delta T_{2\text{pm}}$ difference between GW and FD. Access to groundwater can reduce canopy temperature by up to
334 5°C, in particular when the WTD is shallow. While reductions of 5°C are clearly limited in spatial extent, the overall pattern of
335 cooling associated with groundwater access is quite widespread implying a reduction in heat stress experienced by the woody
336 vegetation during heatwaves. Generally, GW matches MODIS LST better than FD despite the bias in both simulations (compare
337 Figure S6 a-b and Figure S6 c-d). Nevertheless, the temperature reduction between GW and FD is still modest (< 1°C) for most
338 of the forested regions. This may be related to the shallow root distribution assumed in many LSMs, which prevents roots from
339 directly accessing the moisture stored in the deeper soil (note, CABLE assumes 92% of all roots are in the top 64 cm). To
340 examine this possibility, we performed the deep root (DR) sensitivity experiment which prescribed more roots in the deeper soil
341 (56% below 64cm depth). Figure S6e-f illustrates the difference between $\Delta T_{2\text{pm}}$ in DR and $\Delta T_{\text{GW}_2\text{pm}}$. By enabling access to
342 moisture in the deeper soil, the LSM simulates further cooling by 0.2–5°C across the forests. The prescribed deeper roots also
343 lead to an overall better simulation of ΔT at 2 pm relative to the MODIS LST (compare Figure S6g-h with Figure S6a-b).

344

345 Figure 6g-h shows the diurnal cycles of ΔT for the two selected regions (red boxes in Figure 6e-f) compared with the MODIS
346 LST estimated. The region highlighted for the 15th January (Figure 6g) has a WTD of 4–7 m, while the region highlighted for
347 the 25th January (Figure 6h) has a WTD < 4m (Figure S4). In both regions, the simulated ΔT is highest in FD, lower in GW and
348 lowest in DR. Where the WTD is 4–7m (Figure 6g), the three simulated ΔT are slightly lower than ΔT calculated by MODIS
349 LST (red squares). However, in the shallower WTD region (Figure 6h), the simulated ΔT between experiments is more dispersed
350 across experiments and exceeds the MODIS ΔT at both time points, implying that neglecting groundwater dynamics and deep
351 roots is more likely to cause an overestimation of heat stress in the shallower WTD region.

352 3.5 Constraints on groundwater mediation during the compound events

353 We finally probe the reasons for the apparent contradiction between the large impact of groundwater on E during drought
354 (Figure 2a) but a smaller impact on ΔT during the compound events (Figure 6e-f). Figure 7 shows three factors (β , vapour
355 pressure deficit (D) and T_{air}) that constrain the impact of groundwater on ΔT in CABLE during heatwaves in January 2019.
356 Figure 7a shows the difference in ΔT between GW and FD as a function of $\Delta\beta$, suggesting that the inclusion of groundwater
357 has a large impact on ΔT when there is a coincidental and large difference in β between the GW and FD simulations. Figure 7b
358 indicates a clear threshold at $D = 3$ kPa where GW and FD converge, while Figure 7c shows a convergence threshold when the
359 T_{air} exceeds 32°C. Above these two thresholds, access to groundwater seemingly becomes less important in mitigating plant
360 heat stress. There are two mechanisms in CABLE that explain this behaviour. First, as D increases, CABLE predicts that stomata
361 begin to close following a square root dependence (De Kauwe et al., 2015; Medlyn et al., 2011). Second, as T_{air} increases,
362 photosynthesis becomes inhibited as the temperature exceeds the optimum for photosynthesis. In both instances, evaporative
363 cooling is reduced, regardless of the root zone moisture state dictated by groundwater access. That is to say, access to
364 groundwater has limited capacity to directly mediate the heat stress on plants during a compound event when the air is very dry,



365 or very hot.

366 **4 Discussion**

367 In the absence of direct measurements, we used the CABLE-GW LSM, constrained by satellite observations to investigate how
368 groundwater influences ecosystems under conditions of co-occurring droughts and heatwaves. We found that representing
369 groundwater was most important during the onset of drought and the first ~two years of a multi-year drought. This primarily
370 occurred via impeding gravity-driven drainage (Figure 2d) but also via capillary rise from the groundwater aquifer (Figure 2e).
371 This moistening enabled the vegetation to sustain higher E for at least a year (Figure S7).

372

373 When a heatwave occurs during a drought, and in particular early in a drought, the extra transpiration enabled by representing
374 groundwater dynamics helps reduce the heat stress on vegetation (e.g. the reduction of 0.64°C of ΔT over the forests in 2002,
375 Figure 3a). This effect is particularly pronounced in regions with a shallower WTD (e.g. where the groundwater was within the
376 first 5m, there was a 1°C reduction in ΔT in the recent drought, Figure 4d). Importantly, the role played by groundwater
377 diminishes as the drought lengthens beyond two years. Additionally, either the lack of deep roots or stomatal closure caused by
378 high D/T_{air} can reduce the additional transpiration induced by groundwater. The latter plant physiology feedback dominates
379 during heatwaves co-occurring with drought, even if the groundwater's influence has increased root-zone water availability.

380

381 Our results highlight the impact of groundwater on both land surface states (e.g. soil moisture) and on surface fluxes and how
382 this impact varies with the length and intensity of droughts and heatwaves. The results imply that the dominant mechanism by
383 which groundwater buffered transpiration was through impeding gravity-driven drainage. We found a limited role for upward
384 water movement from aquifer due to simulated shallow WTD (which was broadly consistent with the observations in Fan et al.,
385 2013). Further work will be necessary to understand how groundwater interacts with droughts and heatwaves and what these
386 interactions mean for terrestrial ecosystems and the occurrence of the compound extreme events, particularly under the
387 projection of intensifying droughts (Ukkola et al., 2020) and heatwaves (Cowan et al., 2014).

388 **4.1 Changes in the role of groundwater in multi-year droughts**

389 Groundwater is the slowest part of the terrestrial water cycle to change (Condon et al., 2020) and can have a memory of multi-
390 year variations in rainfall (Martínez-de la Torre and Míguez-Macho, 2019; Martinez et al., 2016a). Our results show that the
391 effect of groundwater on the partitioning of available energy between latent and sensible heat fluxes is influenced by the length
392 of drought. As the drought extends in time, the extra E sustained by groundwater decreases (e.g. during the Millennium drought,
393 Figure S7). The role of a drying landscape in modifying the partitioning of available energy between latent and sensible heat
394 fluxes is well known and has been extensively studied (Fan, 2015; Miralles et al., 2019; Seneviratne et al., 2010). Our results
395 add to the knowledge by quantifying the extent of the groundwater control, and eliciting the timescales of influence and the
396 mechanisms at play. The importance of vegetation-groundwater interactions on multi-year timescales has been identified
397 previously. Humphrey et al. (2018) hypothesised that climate models may underestimate the amplitude of global net ecosystem
398 exchange because of a lack of deep-water access. Our regional based results support this hypothesis and in particular highlight
399 the importance of groundwater for explaining the amplitude of fluxes in wet regions (Figure 1), as well as sustaining evaporation
400 during drought.

401 **4.2 Implications for land-atmosphere feedbacks during compound events**

402 Our results show that during drought-heatwave compound events, the existence of groundwater eases the heat stress on the
403 forest canopy and reduces the sensible heat flux to atmosphere. This has the potential to reduce heat accumulating in the



404 boundary layer and help ameliorate the intensity of a heatwave (Keune et al., 2016; Zipper et al., 2019). The presence of
405 groundwater helps dampen a positive feedback loop whereby during drought-heatwave compound events, the high exchange of
406 sensible and low exchange of latent heat can heat the atmosphere and increase the atmospheric demand for water (De Boeck et
407 al., 2010; Massmann et al., 2019), intensifying drying (Miralles et al., 2014). The lack of groundwater in many LSMs suggests
408 a lack of this moderating process and consequently a risk of overestimating the positive feedback in coupled climate simulations.
409 Our results show that neglecting groundwater leads to an average overestimate in canopy temperature by 0.2–1°C where the
410 WTD is shallow (Figure 4d), but as much as 5°C in single heatwave events (Figure 6e-f), leading to an increase in the sensible
411 heat flux (Figure 4e).

412

413 The capacity of groundwater to moderate this positive land-atmosphere feedback is via modifying soil water availability. Firstly,
414 soil water availability influenced by WTD affects how much water is available for E. In the shallow WTD regions, the higher
415 soil water is likely to suppress the mutual enhancement of droughts and heatwaves (Keune et al., 2016; Zipper et al., 2019),
416 particularly early in a drought. However, this suppression becomes weaker as the WTD deepens, in particular at depths beneath
417 the root zone (e.g. 4.6 m in CABLE-GW) or as a drought lengthens. Our results imply the land-amplification of heatwaves is
418 likely stronger in the inland regions (Hirsch et al., 2019) where the WTD is lower than 5m and the influence of groundwater
419 diminishes (Figure S4), and once a drought has intensified significantly.

420

421 On a dry and hot heatwave afternoon, plant physiology feedbacks to high D and high T_{air} dominate transpiration and reduce the
422 influence of groundwater in moderating heatwaves. In CABLE, stomatal closure occurs either directly due to high D (>3 kPa)
423 (De Kauwe et al. 2015) or indirectly due to biochemical feedbacks on photosynthesis at high T_{air} (>32°C) (Kowalczyk et al.,
424 2006); both processes reduce transpiration to near zero, eliminating the buffering effect of groundwater on canopy temperatures.
425 While the timing of the onset of these physiology feedbacks varies across LSMs due to different parameterised sensitivities of
426 stomatal conductance to atmospheric demand (Ball et al., 1987; Leuning et al., 1995) and different temperature dependence
427 parameterisations (Badger and Collatz, 1977; Bernacchi et al., 2001; Crous et al., 2013), importantly, stomatal closure during
428 heat extremes would be model invariant.

429 4.3 Uncertainties and future directions

430 Our study uses a single LSM and consequently the parameterisations included in CABLE-GW influence the quantification of
431 the role of groundwater on droughts and heatwaves. We note CABLE-GW has been extensively evaluated for water cycle
432 processes (Decker, 2015; Decker et al., 2017; Mu et al., 2021; Ukkola et al., 2016b), but evaluation for groundwater interactions
433 remains limited due to the lack of suitable observations (e.g. regional WTD monitoring or detailed knowledge of the distribution
434 of root depths). Figure 1 gives us confidence that CABLE-GW is performing well, based on GRACE data, and other evaluation
435 of CABLE highlights the capacity of CABLE-GW to simulate E well (Decker et al., 2017) but we note here key model
436 parameterisations that may influence the role of groundwater are particularly uncertain.

437

438 We need to be cautious about the “small” groundwater impact on the canopy temperature and associated turbulent energy fluxes
439 during high D or high T_{air} (Figure 3, 4, 6). The thresholds of D and T_{air} currently assumed by LSMs are in fact likely to be
440 species specific. Australian trees in particular have evolved a series of physiological adaptations to reduce the negative impact
441 of heat extremes. It is important to note that most LSMs parameterise their stomatal response to VPD for moderate ranges (< 2
442 kPa), which leads to significant biases at high D (Yang et al., 2019), a feature common in Australia and during heatwaves in
443 general. New theory is needed to ensure that models adequately capture the full range of stomatal response to variability in D
444 (low and high ranges). Similarly, while there is strong evidence to suggest that the optimum temperature for photosynthesis
445 does not vary predictably with the climate of species origin (Kumarathunge et al., 2019) (implying model parameterisations do



446 not need to vary with species), findings from studies do vary (Cunningham and Reed 2002; Reich et al. 2015). Moreover,
447 evidence that plants acclimate their photosynthetic temperature response is strong (Kattge and Knorr, 2007; Kumarathunge et
448 al., 2019; Mercado et al., 2018; Smith et al., 2016; Smith and Dukes, 2013). As a result, it is likely that LSMs currently
449 underestimate groundwater influence during heatwaves due to the interaction with plant physiology feedbacks. This is a key
450 area requiring further investigation. For example, Drake et al. (2018) demonstrated that during a 4-day heatwave > 43°C,
451 Australian *Eucalyptus parramattensis* trees did not reduce transpiration to zero as models would commonly predict, allowing
452 the trees to persist unharmed in a whole-tree chamber experiment. Although De Kauwe et al. (2019) did not find strong support
453 for this phenomenon across eddy covariance sites, if this physiological response is common across Australian woodlands, it
454 would change our view on the importance of soil water availability (therefore groundwater) on the evolution of heatwave or
455 even compound events. Coupled model sensitivity experiments may be important to determine the magnitude that such a
456 physiological feedback would present and could guide the direction of future field/manipulation experiments.

457

458 Root distribution and root function and thereby how roots utilise groundwater are uncertain in models (Arora and Boer, 2003;
459 Drewniak, 2019; Wang et al., 2018; Warren et al., 2015) and indeed in observations (Fan et al., 2017; Jackson et al., 1996;
460 Schenk and Jackson, 2002). Models often ignore how roots forage for water and respond to moisture heterogeneity, limiting the
461 model's ability to accurately reflect the plant usage of groundwater (Warren et al., 2015). In LSMs, roots are typically
462 parameterised using a fixed distribution and normally ignore water uptake from deep roots. This assumption neglects any
463 climatological impact of root distribution and the differentiation in root morphology and function (fine roots vs tap roots),
464 leading to a potential underestimation of groundwater utilization in LSMs (see our deep root experiment, Figure 6g-h). This
465 assumption may be particularly problematic in Australia where vegetation has developed significant adaptation strategies to
466 cope with both extreme heat and drought, including deeply rooted vegetation that can access groundwater (Bartle et al., 1980;
467 Dawson and Pate, 1996; Eamus et al., 2015; Eberbach and Burrows, 2006; Fan et al., 2017). We also note that CABLE does
468 not directly consider hydraulic redistribution, defined as the passive water movement via plant roots from moister to drier soil
469 layers (Burgess et al., 1998; Richards and Caldwell, 1987). Neglecting hydraulic redistribution has the potential to underestimate
470 the groundwater transported upwards and understate the importance of groundwater on ecosystems.

471

472 On the atmosphere side, the existence of groundwater increases the water flux from the land to atmosphere, particularly in
473 regions of shallow WTD, during the first 1–2 years of a drought. This has the potential to moisten the lower atmosphere and
474 may encourage precipitation (Anyah et al., 2008; Jiang et al., 2009; Martinez et al., 2016b; Maxwell et al., 2011). However, our
475 experiments are uncoupled from the atmosphere so while there is the potential for the higher E to affect the boundary layer
476 moisture (Bonetti et al., 2015; Gilbert et al., 2017; Maxwell et al., 2007), clouds and precipitation, we cannot conclude that it
477 would until we undertake future coupled simulations.

478

479 Finally, we note we have focused on the role of groundwater in a natural environment. Humans extract large quantities of
480 groundwater in many regions (Döll et al., 2014; Wada, 2016). Adding human management of groundwater into LSMs enables
481 an examination of how this affects the vulnerability of ecosystems to heatwaves and drought, and may ultimately identify those
482 vulnerable ecosystems close to tipping points that are priorities for protection.

483 5 Conclusions

484 In conclusion, we used the CABLE LSM, constrained by satellite observations, to explore the timescales and extent to which
485 groundwater influences vegetation function and turbulent energy fluxes during multi-year droughts. We showed that
486 groundwater moistened the soil during the first ~two years of a multi-year drought which enabled the vegetation to sustain



487 higher evaporation (50–200 mm yr⁻¹ over the coastal forest regions). This cooled the forest canopy on average by 0.03–0.76 °C
488 and as much as 5 °C in regions of shallow water table depths, helping to moderate the heat stress on vegetation during heatwaves.
489 However, the ability of groundwater to buffer vegetation function varied with the length and intensity of droughts and heatwaves,
490 with its influence decreasing with prolonged drought conditions. Importantly, we also demonstrated that the capacity of the
491 groundwater to buffer evaporative fluxes during heatwaves is dependent on plant physiology feedbacks which regulate stomatal
492 control, irrespective of soil water status. Given increased risk of regional heatwaves and droughts in the future, the role of
493 groundwater on land-atmosphere feedbacks and on terrestrial ecosystems needs to be better understood in order to constrain
494 future projections.

495 **Code and data availability**

496 The CABLE code is available at <https://trac.nci.org.au/trac/cable/wiki> (last access: 30 April 2021) (NCI, 2021) after registration.
497 Here, we use CABLE revision r7765. Scripts for plotting and processing model outputs are available at
498 https://github.com/bibivking/Heatwave/tree/master/GW_DH. GRACE land is available at <http://grace.jpl.nasa.gov>, supported
499 by the NASA MEaSUREs Program. GLEAM dataset is available at <https://www.gleam.eu/>. MOD11A1 MODIS/Terra Land
500 Surface Temperature and the Emissivity Daily L3 Global 1km and MYD11A1 MODIS/Aqua Land Surface Temperature and
501 the Emissivity Daily L3 Global 1km datasets were acquired from the NASA Land Processed Distributed Active Archive Center
502 (LP DAAC), located in the USGS Earth Resources Observation and Science (EROS) Center in Sioux Falls, South Dakota, USA
503 (<https://lpdaacsv.cr.usgs.gov/appears/>).
504

505 **Author contributions**

506 MM, MGDK, AJP and AMU conceived the study, designed the model experiments, investigated the simulations and drafted
507 the manuscript. SH and PRB provided the evaluation and the meteorology forcing datasets. All authors participated in the
508 discussion and revision of the manuscript.
509

510 **Acknowledgements**

511 Mengyuan Mu, Martin G. De Kauwe, Andy J. Pitman, Anna M. Ukkola and Sanaa Hobeichi acknowledge support from the
512 Australian Research Council (ARC) Centre of Excellence for Climate Extremes (CE170100023). Mengyuan Mu acknowledges
513 support from the UNSW University International Postgraduate Award (UIPA) scheme. Martin G. De Kauwe and Andy J. Pitman
514 acknowledge support from the ARC Discovery Grant (DP190101823) and Anna M. Ukkola support from the ARC Discovery
515 Early Career Researcher Award (DE200100086). Martin G. De Kauwe acknowledges support from the NSW Research
516 Attraction and Acceleration Program (RAAP). We thank the National Computational Infrastructure at the Australian National
517 University, an initiative of the Australian Government, for access to supercomputer resources. Mengyuan Mu thanks the
518 University of Nanjing for hosting her research through 2020.
519

520 **References**

521 Abramowitz, G., Leuning, R., Clark, M. and Pitman, A.: Evaluating the performance of land surface models, *J. Clim.*, 21(21),
522 5468–5481, doi:10.1175/2008JCLI2378.1, 2008.



- 523 Allen, C. D., Macalady, A. K., Chenchouni, H., Bachelet, D., McDowell, N., Venetier, M., Kitzberger, T., Rigling, A.,
524 Breshears, D. D., Hogg, E. H. (Ted), Gonzalez, P., Fensham, R., Zhang, Z., Castro, J., Demidova, N., Lim, J.-H., Allard,
525 G., Running, S. W., Semerci, A. and Cobb, N.: A global overview of drought and heat-induced tree mortality reveals
526 emerging climate change risks for forests, *For. Ecol. Manage.*, 259(4), 660–684, doi:10.1016/j.foreco.2009.09.001, 2010.
- 527 Allen, C. D., Breshears, D. D. and McDowell, N. G.: On underestimation of global vulnerability to tree mortality and forest die-
528 off from hotter drought in the Anthropocene, *Ecosphere*, 6(8), art129, doi:10.1890/ES15-00203.1, 2015.
- 529 Anyah, R. O., Weaver, C. P., Miguez-Macho, G., Fan, Y. and Robock, A.: Incorporating water table dynamics in climate
530 modeling: 3. Simulated groundwater influence on coupled land-atmosphere variability, *J. Geophys. Res.*, 113(D7), D07103,
531 doi:10.1029/2007JD009087, 2008.
- 532 Arora, V. K. and Boer, G. J.: A representation of variable root distribution in dynamic vegetation models, *Earth Interact.*, 7(6),
533 1–19, doi:10.1175/1087-3562(2003)007<0001:AROVRD>2.0.CO;2, 2003.
- 534 Badger, M. R. and Collatz, G. J.: Studies on the kinetic mechanism of RuBP carboxylase and oxygenase reactions, with
535 particular reference to the effect of temperature on kinetic parameters, Year book–Carnegie Institution of Washington,
536 Baltimore, Maryland, USA, 355–361 pp., 1977.
- 537 Ball, J. T., Woodrow, I. E. and Berry, J. A.: A model predicting stomatal conductance and its contribution to the control of
538 photosynthesis under different environmental conditions, in *Progress in Photosynthesis Research*, Springer Netherlands,
539 Dordrecht, Netherlands, 221–224 pp., doi:10.1007/978-94-017-0519-6_48, 1987.
- 540 Bartle, G. A., Murray, A. M. and Macpherson, D. K.: The distribution of root length, and the limits to flow of soil water to roots
541 in a dry sclerophyll forest, *For. Sci.*, 26(4), 656–664, doi:10.1093/forestscience/26.4.656, 1980.
- 542 Bernacchi, C. J., Singsaas, E. L., Pimentel, C., Portis Jr, A. R. and Long, S. P.: Improved temperature response functions for
543 models of Rubisco-limited photosynthesis, *Plant. Cell Environ.*, 24(2), 253–259, doi:10.1111/j.1365-3040.2001.00668.x,
544 2001.
- 545 Birami, B., Gattmann, M., Heyer, A. G., Grote, R., Arneht, A. and Ruehr, N. K.: Heat waves alter carbon allocation and increase
546 mortality of Aleppo Pine under dry conditions, *Front. For. Glob. Chang.*, 1, doi:10.3389/ffgc.2018.00008, 2018.
- 547 De Boeck, H. J., Dreesen, F. E., Janssens, I. A. and Nijs, I.: Climatic characteristics of heat waves and their simulation in plant
548 experiments, *Glob. Chang. Biol.*, 16(7), 1992–2000, doi:10.1111/j.1365-2486.2009.02049.x, 2010.
- 549 Bonetti, S., Manoli, G., Domec, J. C., Putti, M., Marani, M. and Katul, G. G.: The influence of water table depth and the free
550 atmospheric state on convective rainfall predisposition, *Water Resour. Res.*, 51(4), 2283–2297,
551 doi:10.1002/2014WR016431, 2015.
- 552 Bureau of Meteorology: Special Climate Statement 43-extreme heat in January 2013. [online] Available from:
553 <http://www.bom.gov.au/climate/current/statements/scs43e.pdf>, 2013.
- 554 Bureau of Meteorology: Special Climate Statement 61-exceptional heat in southeast Australia in early 2017. [online] Available
555 from: <http://www.bom.gov.au/climate/current/statements/scs61.pdf>, 2017.
- 556 Bureau of Meteorology: Special Climate Statement 68—widespread heatwaves during December 2018 and January 2019.
557 [online] Available from: <http://www.bom.gov.au/climate/current/statements/scs68.pdf> (Accessed 18 May 2020), 2019.



- 558 Burgess, S. S. O., Adams, M. A., Turner, N. C. and Ong, C. K.: The redistribution of soil water by tree root systems, *Oecologia*,
559 115(3), 306–311, doi:10.1007/s004420050521, 1998.
- 560 Canadell, J., Jackson, R. B., Ehleringer, J. B., Mooney, H. A., Sala, O. E. and Schulze, E.-D.: Maximum rooting depth of
561 vegetation types at the global scale, *Oecologia*, 108(4), 583–595, doi:10.1007/BF00329030, 1996.
- 562 Ciais, P., Reichstein, M., Viovy, N., Granier, A., Ogee, J., Allard, V., Aubinet, M., Buchmann, N., Bernhofer, C., Carrara, A.,
563 Chevallier, F., De Noblet, N., Friend, A. D., Friedlingstein, P., Grünwald, T., Heinesch, B., Keronen, P., Knohl, A., Krinner,
564 G., Loustau, D., Manca, G., Matteucci, G., Miglietta, F., Ourcival, J. M., Papale, D., Pilegaard, K., Rambal, S., Seufert, G.,
565 Soussana, J. F., Sanz, M. J., Schulze, E. D., Vesala, T. and Valentini, R.: Europe-wide reduction in primary productivity
566 caused by the heat and drought in 2003, *Nature*, 437(7058), 529–533, doi:10.1038/nature03972, 2005.
- 567 Condon, L. E., Atchley, A. L. and Maxwell, R. M.: Evapotranspiration depletes groundwater under warming over the contiguous
568 United States, *Nat. Commun.*, 11(1), 873, doi:10.1038/s41467-020-14688-0, 2020.
- 569 Cowan, T., Purich, A., Perkins, S., Pezza, A., Boschat, G. and Sadler, K.: More frequent, longer, and hotter heat waves for
570 Australia in the twenty-first century, *J. Clim.*, 27(15), 5851–5871, doi:10.1175/JCLI-D-14-00092.1, 2014.
- 571 Crous, K. Y., Quentin, A. G., Lin, Y.-S., Medlyn, B. E., Williams, D. G., Barton, C. V. M. and Ellsworth, D. S.: Photosynthesis
572 of temperate *Eucalyptus globulus* trees outside their native range has limited adjustment to elevated CO₂ and climate
573 warming, *Glob. Chang. Biol.*, 19(12), 3790–3807, doi:10.1111/gcb.12314, 2013.
- 574 D’Odorico, P. and Porporato, A.: Preferential states in soil moisture and climate dynamics, *Proc. Natl. Acad. Sci.*, 101(24),
575 8848–8851, doi:10.1073/pnas.0401428101, 2004.
- 576 Dawson, T. E. and Pate, J. S.: Seasonal water uptake and movement in root systems of Australian phreatophytic plants of
577 dimorphic root morphology: a stable isotope investigation, *Oecologia*, 107(1), 13–20, doi:10.1007/BF00582230, 1996.
- 578 Decker, M.: Development and evaluation of a new soil moisture and runoff parameterization for the CABLE LSM including
579 subgrid-scale processes, *J. Adv. Model. Earth Syst.*, 7(4), 1788–1809, doi:10.1002/2015MS000507, 2015.
- 580 Decker, M., Or, D., Pitman, A. and Ukkola, A.: New turbulent resistance parameterization for soil evaporation based on a pore-
581 scale model: Impact on surface fluxes in CABLE, *J. Adv. Model. Earth Syst.*, 9(1), 220–238, doi:10.1002/2016MS000832,
582 2017.
- 583 van Dijk, A. I. J. M., Beck, H. E., Crosbie, R. S., de Jeu, R. A. M., Liu, Y. Y., Podger, G. M., Timbal, B. and Viney, N.
584 R.: The Millennium Drought in southeast Australia (2001-2009): Natural and human causes and implications for water
585 resources, ecosystems, economy, and society, *Water Resour. Res.*, 49(2), 1040–1057, doi:10.1002/wrcr.20123, 2013.
- 586 Döll, P., Müller Schmied, H., Schuh, C., Portmann, F. T. and Eicker, A.: Global-scale assessment of groundwater depletion and
587 related groundwater abstractions: Combining hydrological modeling with information from well observations and GRACE
588 satellites, *Water Resour. Res.*, 50(7), 5698–5720, doi:10.1002/2014WR015595, 2014.
- 589 Drake, J. E., Tjoelker, M. G., Vårhammar, A., Medlyn, B. E., Reich, P. B., Leigh, A., Pfautsch, S., Blackman, C. J., López, R.,
590 Aspinwall, M. J., Crous, K. Y., Duursma, R. A., Kumarathunge, D., De Kauwe, M. G., Jiang, M., Nicotra, A. B., Tissue,
591 D. T., Choat, B., Atkin, O. K. and Barton, C. V. M. M.: Trees tolerate an extreme heatwave via sustained transpirational
592 cooling and increased leaf thermal tolerance, *Glob. Chang. Biol.*, 24(6), 2390–2402, doi:10.1111/gcb.14037, 2018.



- 593 DREWNIAK, B. A.: Simulating dynamic roots in the energy exascale earth system land model, *J. Adv. Model. Earth Syst.*, 11(1),
594 338–359, doi:10.1029/2018MS001334, 2019.
- 595 EAMUS, D. and FROEND, R.: Groundwater-dependent ecosystems: the where, what and why of GDEs, *Aust. J. Bot.*, 54(2), 91,
596 doi:10.1071/BT06029, 2006.
- 597 EAMUS, D., ZOLFAGHAR, S., VILLALOBOS-VEGA, R., CLEVERLY, J. and HUETE, A.: Groundwater-dependent ecosystems: recent insights
598 from satellite and field-based studies, *Hydrol. Earth Syst. Sci.*, 19(10), 4229–4256, doi:10.5194/hess-19-4229-2015, 2015.
- 599 EBERBACH, P. L. and BURROWS, G. E.: The transpiration response by four topographically distributed Eucalyptus species, to
600 rainfall occurring during drought in south eastern Australia, *Physiol. Plant.*, 127(3), 483–493, doi:10.1111/j.1399-
601 3054.2006.00762.x, 2006.
- 602 FAN, Y.: Groundwater in the Earth’s critical zone: Relevance to large-scale patterns and processes, *Water Resour. Res.*, 51(5),
603 3052–3069, doi:10.1002/2015WR017037, 2015.
- 604 FAN, Y., LI, H. and MIGUEZ-MACHO, G.: Global patterns of groundwater table depth, *Science*, 339(6122), 940–943,
605 doi:10.1126/science.1229881, 2013.
- 606 FAN, Y., MIGUEZ-MACHO, G., JOBBÁGY, E. G., JACKSON, R. B. and OTERO-CASAL, C.: Hydrologic regulation of plant rooting depth,
607 *Proc. Natl. Acad. Sci.*, 114(40), 10572–10577, doi:10.1073/pnas.1712381114, 2017.
- 608 FISCHER, E. M., SENEVIRATNE, S. I., VIDALE, P. L., LÜTHI, D. and SCHÄR, C.: Soil moisture–atmosphere interactions during the 2003
609 European summer heat wave, *J. Clim.*, 20(20), 5081–5099, doi:10.1175/JCLI4288.1, 2007.
- 610 GALE, M. R. and GRIGAL, D. F.: Vertical root distributions of northern tree species in relation to successional status, *Can. J. For.*
611 *Res.*, 17(8), 829–834, doi:10.1139/x87-131, 1987.
- 612 GEANGE, S. R., ARNOLD, P. A., CATLING, A. A., COAST, O., COOK, A. M., GOWLAND, K. M., LEIGH, A., NOTARNICOLA, R. F., POSCH, B.
613 C., VENN, S. E., ZHU, L. and NICOTRA, A. B.: The thermal tolerance of photosynthetic tissues: a global systematic review
614 and agenda for future research, *New Phytol.*, 229(5), 2497–2513, doi:10.1111/nph.17052, 2021.
- 615 GILBERT, J. M., MAXWELL, R. M. and GOCHIS, D. J.: Effects of water-table configuration on the planetary boundary layer over the
616 San Joaquin River Watershed, California, *J. Hydrometeorol.*, 18(5), 1471–1488, doi:10.1175/JHM-D-16-0134.1, 2017.
- 617 GRIFFITH, S. J., BALE, C. and ADAM, P.: Environmental correlates of coastal heathland and allied vegetation, *Aust. J. Bot.*, 56(6),
618 512, doi:10.1071/BT06147, 2008.
- 619 HAVERD, V., RAUPACH, M. R., BRIGGS, P. R., CANADELL, J. G., ISAAC, P., PICKETT-HEAPS, C., ROXBURGH, S. H., VAN GORSEL, E., VISCARRA
620 ROSSEL, R. A. and WANG, Z.: Multiple observation types reduce uncertainty in Australia’s terrestrial carbon and water cycles,
621 *Biogeosciences*, 10(3), 2011–2040, doi:10.5194/bg-10-2011-2013, 2013.
- 622 HENGL, T., MENDES DE JESUS, J., HEUVELINK, G. B. M., RUIPEREZ GONZALEZ, M., KILIBARDA, M., BLAGOTIĆ, A., SHANGGUAN, W.,
623 WRIGHT, M. N., GENG, X., BAUER-MARSCHALLINGER, B., GUEVARA, M. A., VARGAS, R., MACMILLAN, R. A., BATJES, N. H., LEENAARS,
624 J. G. B., RIBEIRO, E., WHEELER, I., MANTEL, S. and KEMPEN, B.: SoilGrids250m: Global gridded soil information based on
625 machine learning, edited by B. Bond-Lamberty, *PLoS One*, 12(2), e0169748, doi:10.1371/journal.pone.0169748, 2017.
- 626 HIRSCH, A. L., EVANS, J. P., DI VIRGILIO, G., PERKINS-KIRKPATRICK, S. E., ARGÜESO, D., PITMAN, A. J., CAROUGE, C. C., KALA, J.,
627 ANDRYS, J., PETRELLI, P. and ROCKEL, B.: Amplification of Australian heatwaves via local land-atmosphere coupling, *J.*
628 *Geophys. Res. Atmos.*, 124(24), 13625–13647, doi:10.1029/2019JD030665, 2019.



- 629 Horton, R. M., Mankin, J. S., Lesk, C., Coffel, E. and Raymond, C.: A review of recent advances in research on extreme heat
630 events, *Curr. Clim. Chang. Reports*, 2(4), 242–259, doi:10.1007/s40641-016-0042-x, 2016.
- 631 Humphrey, V., Zscheischler, J., Ciais, P., Gudmundsson, L., Sitch, S. and Seneviratne, S. I.: Sensitivity of atmospheric CO₂
632 growth rate to observed changes in terrestrial water storage, *Nature*, 560(7720), 628–631, doi:10.1038/s41586-018-0424-
633 4, 2018.
- 634 Ibáñez, I., Acharya, K., Juno, E., Karounos, C., Lee, B. R., McCollum, C., Schaffer-Morrison, S. and Tourville, J.: Forest
635 resilience under global environmental change: Do we have the information we need? A systematic review, edited by R.
636 Zang, *PLoS One*, 14(9), e0222207, doi:10.1371/journal.pone.0222207, 2019.
- 637 Jackson, R. B., Canadell, J., Ehleringer, J. R., Mooney, H. A., Sala, O. E. and Schulze, E. D.: A global analysis of root
638 distributions for terrestrial biomes, *Oecologia*, 108(3), 389–411, doi:10.1007/BF00333714, 1996.
- 639 Jiang, X., Niu, G.-Y. and Yang, Z.-L.: Impacts of vegetation and groundwater dynamics on warm season precipitation over the
640 Central United States, *J. Geophys. Res.*, 114(D6), D06109, doi:10.1029/2008JD010756, 2009.
- 641 Jones, D., Wang, W. and Fawcett, R.: High-quality spatial climate data-sets for Australia, *Aust. Meteorol. Oceanogr. J.*, 58(04),
642 233–248, doi:10.22499/2.5804.003, 2009.
- 643 Jyoteeshkumar reddy, P., Sharples, J. J., Lewis, S. C. and Perkins-Kirkpatrick, S. E.: Modulating influence of drought on the
644 synergy between heatwaves and dead fine fuel moisture content of bushfire fuels in the Southeast Australian region,
645 *Weather Clim. Extrem.*, 31, 100300, doi:10.1016/j.wace.2020.100300, 2021.
- 646 Kattge, J. and Knorr, W.: Temperature acclimation in a biochemical model of photosynthesis: a reanalysis of data from 36
647 species, *Plant. Cell Environ.*, 30(9), 1176–1190, doi:10.1111/j.1365-3040.2007.01690.x, 2007.
- 648 De Kauwe, M. G., Kala, J., Lin, Y. S., Pitman, A. J., Medlyn, B. E., Duursma, R. A., Abramowitz, G., Wang, Y. P. and Miralles,
649 D. G.: A test of an optimal stomatal conductance scheme within the CABLE land surface model, *Geosci. Model Dev.*, 8(2),
650 431–452, doi:10.5194/gmd-8-431-2015, 2015.
- 651 De Kauwe, M. G., Medlyn, B. E., Pitman, A. J., Drake, J. E., Ukkola, A., Griebel, A., Pendall, E., Prober, S. and Roderick, M.:
652 Examining the evidence for decoupling between photosynthesis and transpiration during heat extremes, *Biogeosciences*,
653 16(4), 903–916, doi:10.5194/bg-16-903-2019, 2019.
- 654 De Kauwe, M. G., Medlyn, B. E., Ukkola, A. M., Mu, M., Sabot, M. E. B. B., Pitman, A. J., Meir, P., Cernusak, L. A., Rifai, S.
655 W., Choat, B., Tissue, D. T., Blackman, C. J., Li, X., Roderick, M. and Briggs, P. R.: Identifying areas at risk of drought-
656 induced tree mortality across South-Eastern Australia, *Glob. Chang. Biol.*, 26(10), 5716–5733, doi:10.1111/gcb.15215,
657 2020.
- 658 Keune, J., Gasper, F., Goergen, K., Hense, A., Shrestha, P., Sulis, M. and Kollet, S.: Studying the influence of groundwater
659 representations on land surface-atmosphere feedbacks during the European heat wave in 2003, *J. Geophys. Res. Atmos.*,
660 121(22), 13,301–13,325, doi:10.1002/2016JD025426, 2016.
- 661 Kim, W., Iizumi, T. and Nishimori, M.: Global Patterns of Crop Production Losses Associated with Droughts from 1983 to
662 2009, *J. Appl. Meteorol. Climatol.*, 58(6), 1233–1244, doi:10.1175/JAMC-D-18-0174.1, 2019.



- 663 Kowalczyk, E. A., Wang, Y. P. and Law, R. M.: The CSIRO Atmosphere Biosphere Land Exchange (CABLE) model for use
664 in climate models and as an offline model, *CSIRO Mar. Atmos. Res. Pap.*, 13(November 2015), 1–42,
665 doi:10.4225/08/58615c6a9a51d, 2006.
- 666 Kuginis, L., Dabovic, J., Burne, G., Raine, A. and Hemakumara, H.: Methods for the identification of high probability
667 groundwater dependent vegetation ecosystems, *DPI Water: Sydney, NSW*. [online] Available from: www.dpi.nsw.gov.au,
668 2016.
- 669 Kumarathunge, D. P., Medlyn, B. E., Drake, J. E., Tjoelker, M. G., Aspinwall, M. J., Battaglia, M., Cano, F. J., Carter, K. R.,
670 Cavaleri, M. A., Cernusak, L. A., Chambers, J. Q., Crous, K. Y., De Kauwe, M. G., Dillaway, D. N., Dreyer, E., Ellsworth,
671 D. S., Ghannoum, O., Han, Q., Hikosaka, K., Jensen, A. M., Kelly, J. W. G. G., Kruger, E. L., Mercado, L. M., Onoda, Y.,
672 Reich, P. B., Rogers, A., Slot, M., Smith, N. G., Tarvainen, L., Tissue, D. T., Togashi, H. F., Tribuzy, E. S., Uddling, J.,
673 Vårhammar, A., Wallin, G., Warren, J. M. and Way, D. A.: Acclimation and adaptation components of the temperature
674 dependence of plant photosynthesis at the global scale, *New Phytol.*, 222(2), 768–784, doi:10.1111/nph.15668, 2019.
- 675 Landerer, F. W., Flechtner, F. M., Save, H., Webb, F. H., Bandikova, T., Bertiger, W. I., Bettadpur, S. V., Byun, S. H., Dahle,
676 C., Dobslaw, H., Fahnestock, E., Harvey, N., Kang, Z., Kruizinga, G. L. H., Loomis, B. D., McCullough, C., Murböck,
677 M., Nagel, P., Paik, M., Pie, N., Poole, S., Strelakov, D., Tamisiea, M. E., Wang, F., Watkins, M. M., Wen, H., Wiese, D.
678 N. and Yuan, D.: Extending the global mass change data record: GRACE Follow-On instrument and science data
679 performance, *Geophys. Res. Lett.*, 47(12), doi:10.1029/2020GL088306, 2020.
- 680 Leblanc, M. J., Tregoning, P., Ramillien, G., Tweed, S. O. and Fakes, A.: Basin-scale, integrated observations of the early 21st
681 century multiyear drought in southeast Australia, *Water Resour. Res.*, 45(4), 1–10, doi:10.1029/2008WR007333, 2009.
- 682 Lesk, C., Rowhani, P. and Ramankutty, N.: Influence of extreme weather disasters on global crop production, *Nature*, 529(7584),
683 84–87, doi:10.1038/nature16467, 2016.
- 684 Leuning, R., Kelliher, F. M., Pury, D. G. G. and Schulze, E.-D.: Leaf nitrogen, photosynthesis, conductance and transpiration:
685 scaling from leaves to canopies, *Plant, Cell Environ.*, 18(10), 1183–1200, doi:10.1111/j.1365-3040.1995.tb00628.x, 1995.
- 686 Marchionni, V., Daly, E., Manoli, G., Tapper, N. J., Walker, J. P. and Fatichi, S.: Groundwater buffers drought effects and
687 climate variability in urban reserves, *Water Resour. Res.*, 56(5), doi:10.1029/2019WR026192, 2020.
- 688 Martens, B., Miralles, D. G., Lievens, H., van der Schalie, R., de Jeu, R. A. M., Fernández-Prieto, D., Beck, H. E., Dorigo, W.
689 A. and Verhoest, N. E. C. C.: GLEAM v3: satellite-based land evaporation and root-zone soil moisture, *Geosci. Model
690 Dev.*, 10(5), 1903–1925, doi:10.5194/gmd-10-1903-2017, 2017.
- 691 Martínez-de la Torre, A. and Miguez-Macho, G.: Groundwater influence on soil moisture memory and land–atmosphere fluxes
692 in the Iberian Peninsula, *Hydrol. Earth Syst. Sci.*, 23(12), 4909–4932, doi:10.5194/hess-23-4909-2019, 2019.
- 693 Martínez, J. A., Dominguez, F. and Miguez-Macho, G.: Effects of a groundwater scheme on the simulation of soil moisture and
694 evapotranspiration over southern South America, *J. Hydrometeorol.*, 17(11), 2941–2957, doi:10.1175/JHM-D-16-0051.1,
695 2016a.
- 696 Martínez, J. A., Dominguez, F. and Miguez-Macho, G.: Impacts of a groundwater scheme on hydroclimatological conditions
697 over southern South America, *J. Hydrometeorol.*, 17(11), 2959–2978, doi:10.1175/JHM-D-16-0052.1, 2016b.
- 698 Massmann, A., Gentine, P. and Lin, C.: When does vapor pressure deficit drive or reduce evapotranspiration?, *J. Adv. Model.
699 Earth Syst.*, 11(10), 3305–3320, doi:10.1029/2019MS001790, 2019.



- 700 Maxwell, R. M., Chow, F. K. and Kollet, S. J.: The groundwater–land-surface–atmosphere connection: Soil moisture effects on
701 the atmospheric boundary layer in fully-coupled simulations, *Adv. Water Resour.*, 30(12), 2447–2466,
702 doi:10.1016/j.advwatres.2007.05.018, 2007.
- 703 Maxwell, R. M., Lundquist, J. K., Mirocha, J. D., Smith, S. G., Woodward, C. S. and Tompson, A. F. B.: Development of a
704 coupled groundwater–atmosphere model, *Mon. Weather Rev.*, 139(1), 96–116, doi:10.1175/2010MWR3392.1, 2011.
- 705 McVicar, T. R., Van Niel, T. G., Li, L. T., Roderick, M. L., Rayner, D. P., Ricciardulli, L. and Donohue, R. J.: Wind speed
706 climatology and trends for Australia, 1975–2006: Capturing the stilling phenomenon and comparison with near-surface
707 reanalysis output, *Geophys. Res. Lett.*, 35(20), 1–6, doi:10.1029/2008GL035627, 2008.
- 708 Medlyn, B. E., Duursma, R. A., Eamus, D., Ellsworth, D. S., Prentice, C. I., Barton, C. V. M., Crous, K. Y., De Angelis, P.,
709 Freeman, M. and Wingate, L.: Reconciling the optimal and empirical approaches to modelling stomatal conductance, *Glob.
710 Chang. Biol.*, 17(6), 2134–2144, doi:10.1111/j.1365-2486.2010.02375.x, 2011.
- 711 Mercado, L. M., Medlyn, B. E., Huntingford, C., Oliver, R. J., Clark, D. B., Sitch, S., Zelazowski, P., Kattge, J., Harper, A. B.
712 and Cox, P. M.: Large sensitivity in land carbon storage due to geographical and temporal variation in the thermal response
713 of photosynthetic capacity, *New Phytol.*, 218(4), 1462–1477, doi:10.1111/nph.15100, 2018.
- 714 Miller, G. R., Chen, X., Rubin, Y., Ma, S. and Baldocchi, D. D.: Groundwater uptake by woody vegetation in a semiarid oak
715 savanna, *Water Resour. Res.*, 46(10), 2009WR008902, doi:10.1029/2009WR008902, 2010.
- 716 Miralles, D. G., Holmes, T. R. H. H., De Jeu, R. A. M. M., Gash, J. H., Meesters, A. G. C. A. C. A. and Dolman, A. J.: Global
717 land-surface evaporation estimated from satellite-based observations, *Hydrol. Earth Syst. Sci.*, 15(2), 453–469,
718 doi:10.5194/hess-15-453-2011, 2011.
- 719 Miralles, D. G., Teuling, A. J., van Heerwaarden, C. C. and Vilà-Guerau de Arellano, J.: Mega-heatwave temperatures due to
720 combined soil desiccation and atmospheric heat accumulation, *Nat. Geosci.*, 7(5), 345–349, doi:10.1038/ngeo2141, 2014.
- 721 Miralles, D. G., Gentine, P., Seneviratne, S. I. and Teuling, A. J.: Land-atmospheric feedbacks during droughts and heatwaves:
722 state of the science and current challenges, *Ann. N. Y. Acad. Sci.*, 1436(1), 19–35, doi:10.1111/nyas.13912, 2019.
- 723 Mitchell, P. J., O’Grady, A. P., Hayes, K. R. and Pinkard, E. A.: Exposure of trees to drought-induced die-off is defined by a
724 common climatic threshold across different vegetation types, *Ecol. Evol.*, 4(7), 1088–1101, doi:10.1002/ece3.1008, 2014.
- 725 Mu, M., De Kauwe, M. G., Ukkola, A. M., Pitman, A. J., Gimeno, T. E., Medlyn, B. E., Or, D., Yang, J. and Ellsworth, D. S.:
726 Evaluating a land surface model at a water-limited site: implications for land surface contributions to droughts and
727 heatwaves, *Hydrol. Earth Syst. Sci.*, 25(1), 447–471, doi:10.5194/hess-25-447-2021, 2021.
- 728 Mukherjee, S., Ashfaq, M. and Mishra, A. K.: Compound Drought and Heatwaves at a Global Scale: The role of natural climate
729 variability-associated synoptic patterns and land-surface energy budget anomalies, *J. Geophys. Res. Atmos.*, 125(11),
730 doi:10.1029/2019JD031943, 2020.
- 731 Nairn, J. R. and Fawcett, R. J. B.: The excess heat factor: A metric for heatwave intensity and its use in classifying heatwave
732 severity, *Int. J. Environ. Res. Public Health*, 12(1), 227–253, doi:10.3390/ijerph120100227, 2014.
- 733 National Climate Centre: The exceptional January-February 2009 heatwave in south-eastern Australia. [online] Available from:
734 <http://www.bom.gov.au/climate/current/statements/scs17c.pdf>, 2009.



- 735 NCI: CABLE: The Community Atmosphere Biosphere Land Ex- change Model, available at: <https://trac.nci.org.au/trac/cable/>
736 wiki, last access: 30 April 2021.
- 737 O'sullivan, O. S., Heskel, M. A., Reich, P. B., Tjoelker, M. G., Weerasinghe, L. K., Penillard, A., Zhu, L., Egerton, J. J. G.,
738 Bloomfield, K. J., Creek, D. and others: Thermal limits of leaf metabolism across biomes, *Glob. Chang. Biol.*, 23(1), 209–
739 223, 2017.
- 740 Orth, R. and Destouni, G.: Drought reduces blue-water fluxes more strongly than green-water fluxes in Europe, *Nat. Commun.*,
741 9(1), 3602, doi:10.1038/s41467-018-06013-7, 2018.
- 742 Perkins-Kirkpatrick, S. E., White, C. J., Alexander, L. V., Argüeso, D., Boschat, G., Cowan, T., Evans, J. P., Ekström, M., Oliver,
743 E. C. J., Phatak, A. and Purich, A.: Natural hazards in Australia: heatwaves, *Clim. Change*, 139(1), 101–114,
744 doi:10.1007/s10584-016-1650-0, 2016.
- 745 Perkins, S. E.: A review on the scientific understanding of heatwaves—Their measurement, driving mechanisms, and changes
746 at the global scale, *Atmos. Res.*, 164–165, 242–267, doi:10.1016/j.atmosres.2015.05.014, 2015.
- 747 Raupach, M. R.: Simplified expressions for vegetation roughness length and zero-plane displacement as functions of canopy
748 height and area index, *Boundary-Layer Meteorol.*, 71(1–2), 211–216, doi:10.1007/BF00709229, 1994.
- 749 Raupach, M. R., Finkelde, K. and Zhang, L.: SCAM: a soil-canopy-atmosphere model: description and comparisons with field
750 data, CSIRO Centre for Environmental Mechanics, Canberra, Australia, <https://doi.org/10.4225/08/5a30195883b8f>, 1997.
- 751 Raupach, M. R., Haverd, V. and Briggs, P. R.: Sensitivities of the Australian terrestrial water and carbon balances to climate
752 change and variability, *Agric. For. Meteorol.*, 182–183, 277–291, doi:10.1016/j.agrformet.2013.06.017, 2013.
- 753 Richards, J. H. and Caldwell, M. M.: Hydraulic lift: Substantial nocturnal water transport between soil layers by *Artemisia*
754 *tridentata* roots, *Oecologia*, 73(4), 486–489, doi:10.1007/BF00379405, 1987.
- 755 Ruehr, N. K., Grote, R., Mayr, S. and Arneith, A.: Beyond the extreme: recovery of carbon and water relations in woody plants
756 following heat and drought stress, *Tree Physiol.*, 39(8), 1285–1299, doi:10.1093/treephys/tpz032, 2019.
- 757 Sandi, S. G., Rodriguez, J. F., Saintilan, N., Wen, L., Kuczera, G., Riccardi, G. and Saco, P. M.: Resilience to drought of dryland
758 wetlands threatened by climate change, *Sci. Rep.*, 10(1), 13232, doi:10.1038/s41598-020-70087-x, 2020.
- 759 Schenk, H. J. and Jackson, R. B.: The global biogeography of roots, *Ecol. Monogr.*, 72(3), 311–328,
760 doi:[https://doi.org/10.1890/0012-9615\(2002\)072\[0311:TGBOR\]2.0.CO;2](https://doi.org/10.1890/0012-9615(2002)072[0311:TGBOR]2.0.CO;2), 2002.
- 761 Schumacher, D. L., Keune, J., van Heerwaarden, C. C., Vilà-Guerau de Arellano, J., Teuling, A. J. and Miralles, D. G.:
762 Amplification of mega-heatwaves through heat torrents fuelled by upwind drought, *Nat. Geosci.*, 12(9), 712–717,
763 doi:10.1038/s41561-019-0431-6, 2019.
- 764 Seneviratne, S. I., Corti, T., Davin, E. L., Hirschi, M., Jaeger, E. B., Lehner, I., Orlowsky, B. and Teuling, A. J.: Investigating
765 soil moisture–climate interactions in a changing climate: A review, *Earth-Science Rev.*, 99(3–4), 125–161,
766 doi:10.1016/j.earscirev.2010.02.004, 2010.
- 767 Shrestha, P., Sulis, M., Masbou, M., Kollet, S. and Simmer, C.: A scale-consistent terrestrial systems modeling platform based
768 on COSMO, CLM, and ParFlow, *Mon. Weather Rev.*, 142(9), 3466–3483, doi:10.1175/MWR-D-14-00029.1, 2014.



- 769 Smith, N. G. and Dukes, J. S.: Plant respiration and photosynthesis in global-scale models: incorporating acclimation to
770 temperature and CO₂, *Glob. Chang. Biol.*, 19(1), 45–63, doi:10.1111/j.1365-2486.2012.02797.x, 2013.
- 771 Smith, N. G., Malyshev, S. L., Shevliakova, E., Kattge, J. and Dukes, J. S.: Foliar temperature acclimation reduces simulated
772 carbon sensitivity to climate, *Nat. Clim. Chang.*, 6(4), 407–411, doi:10.1038/nclimate2878, 2016.
- 773 Swenson, S. C. and Lawrence, D. M.: Assessing a dry surface layer-based soil resistance parameterization for the Community
774 Land Model using GRACE and FLUXNET-MTE data, *J. Geophys. Res. Atmos.*, 119(17), 10,299–10,312,
775 doi:10.1002/2014JD022314, 2014.
- 776 Teuling, A. J., Van Loon, A. F., Seneviratne, S. I., Lehner, I., Aubinet, M., Heinesch, B., Bernhofer, C., Grünwald, T., Prasse,
777 H. and Spank, U.: Evapotranspiration amplifies European summer drought, *Geophys. Res. Lett.*, 40(10), 2071–2075,
778 doi:10.1002/grl.50495, 2013.
- 779 Thorburn, P. J., Walker, G. R. and Woods, P. H.: Comparison of diffuse discharge from shallow water tables in soils and salt
780 flats, *J. Hydrol.*, 136(1–4), 253–274, doi:10.1016/0022-1694(92)90014-M, 1992.
- 781 Trudinger, C. M., Haverd, V., Briggs, P. R. and Canadell, J. G.: Interannual variability in Australia’s terrestrial carbon cycle
782 constrained by multiple observation types, *Biogeosciences*, 13(23), 6363–6383, doi:10.5194/bg-13-6363-2016, 2016.
- 783 Trugman, A. T., Medvigy, D., Mankin, J. S. and Anderegg, W. R. L.: Soil moisture stress as a major driver of carbon cycle
784 uncertainty, *Geophys. Res. Lett.*, 45(13), 6495–6503, doi:10.1029/2018GL078131, 2018.
- 785 Ukkola, A. M., De Kauwe, M. G., Pitman, A. J., Best, M. J., Abramowitz, G., Haverd, V., Decker, M. and Haughton, N.: Land
786 surface models systematically overestimate the intensity, duration and magnitude of seasonal-scale evaporative droughts,
787 *Environ. Res. Lett.*, 11(10), 104012, doi:10.1088/1748-9326/11/10/104012, 2016a.
- 788 Ukkola, A. M., Pitman, A. J., Decker, M., De Kauwe, M. G., Abramowitz, G., Kala, J. and Wang, Y.-P.: Modelling
789 evapotranspiration during precipitation deficits: identifying critical processes in a land surface model, *Hydrol. Earth Syst.
790 Sci.*, 20(6), 2403–2419, doi:10.5194/hess-20-2403-2016, 2016b.
- 791 Ukkola, A. M., De Kauwe, M. G., Roderick, M. L., Abramowitz, G. and Pitman, A. J.: Robust future changes in meteorological
792 drought in CMIP6 projections despite uncertainty in precipitation, *Geophys. Res. Lett.*, 47(11), e2020GL087820,
793 doi:10.1029/2020GL087820, 2020.
- 794 Verdon-Kidd, D. C. and Kiem, A. S.: Nature and causes of protracted droughts in southeast Australia: Comparison between the
795 Federation, WWII, and Big Dry droughts, *Geophys. Res. Lett.*, 36(22), L22707, doi:10.1029/2009GL041067, 2009.
- 796 Wada, Y.: Impacts of groundwater pumping on regional and global water resources, in: *Terrestrial Water Cycle and Climate
797 Change*, American Geophysical Union, edited by: Tang, Q. and Oki, T., Hoboken, United States, 71–101, doi:
798 10.1002/9781118971772.ch5, 2016.
- 799 Wan Z.: MOD11A1 MODIS/Terra Land Surface Temperature and the Emissivity Daily L3 Global 1km SIN Grid, NASA LP
800 DAAC, <http://doi.org/10.5067/MODIS/MOD11A1.006>, 2015a. Last access: 14 April 2021.
- 801 Wan Z.: MYD11A1 MODIS/Aqua Land Surface Temperature and the Emissivity Daily L3 Global 1km SIN Grid, NASA LP
802 DAAC, <http://doi.org/10.5067/MODIS/MYD11A1.006>, 2015b. Last access: 14 April 2021.
- 803 Wan, Z. and Li, Z.-L.: A physics-based algorithm for retrieving land-surface emissivity and temperature from EOS/MODIS
804 data, *IEEE Trans. Geosci. Remote Sens.*, 35(4), 980–996, doi:10.1109/36.602541, 1997.



- 805 Wang, K. and Dickinson, R. E.: A review of global terrestrial evapotranspiration: Observation, modeling, climatology, and
806 climatic variability, *Rev. Geophys.*, 50(2), doi:10.1029/2011RG000373, 2012.
- 807 Wang, P., Niu, G., Fang, Y., Wu, R., Yu, J., Yuan, G., Pozdniakov, S. P. and Scott, R. L.: Implementing dynamic root
808 optimization in Noah-MP for simulating phreatophytic root water uptake, *Water Resour. Res.*, 54(3), 1560–1575,
809 doi:10.1002/2017WR021061, 2018.
- 810 Wang, Y.-P. and Leuning, R.: A two-leaf model for canopy conductance, photosynthesis and partitioning of available energy I:
811 Model description and comparison with a multi-layered model, *Agric. For. Meteorol.*, 91(1–2), 89–111,
812 doi:10.1016/S0168-1923(98)00061-6, 1998.
- 813 Wang, Y. P., Kowalczyk, E., Leuning, R., Abramowitz, G., Raupach, M. R., Pak, B., van Gorsel, E. and Luhr, A.: Diagnosing
814 errors in a land surface model (CABLE) in the time and frequency domains, *J. Geophys. Res.*, 116(G1), G01034,
815 doi:10.1029/2010JG001385, 2011.
- 816 Warren, J. M., Hanson, P. J., Iversen, C. M., Kumar, J., Walker, A. P. and Wullschleger, S. D.: Root structural and functional
817 dynamics in terrestrial biosphere models - evaluation and recommendations, *New Phytol.*, 205(1), 59–78,
818 doi:10.1111/nph.13034, 2015.
- 819 Watkins, M. M., Wiese, D. N., Yuan, D.-N., Boening, C. and Landerer, F. W.: Improved methods for observing Earth's time
820 variable mass distribution with GRACE using spherical cap mascons, *J. Geophys. Res. Solid Earth*, 120(4), 2648–2671,
821 doi:10.1002/2014JB011547, 2015.
- 822 Wiese, D. N., Landerer, F. W. and Watkins, M. M.: Quantifying and reducing leakage errors in the JPL RL05M GRACE mascon
823 solution, *Water Resour. Res.*, 52(9), 7490–7502, doi:10.1002/2016WR019344, 2016.
- 824 Wiese, D. N., Yuan, D.-N., Boening, C., Landerer, F. W., Watkins, M. M.: JPL GRACE Mascon Ocean, Ice, and Hydrology
825 Equivalent Water Height Release 06 Coastal Resolution Improvement (CRI) Filtered Version 1.0. Ver. 1.0., PO.DAAC,
826 CA, USA. <http://dx.doi.org/10.5067/TEMSC-3MJC6>, 2018. Last access: 14 April 2021.
- 827 Yang, J., Duursma, R. A., De Kauwe, M. G., Kumarathunge, D., Jiang, M., Mahmud, K., Gimeno, T. E., Crous, K. Y., Ellsworth,
828 D. S., Peters, J., Choat, B., Eamus, D. and Medlyn, B. E.: Incorporating non-stomatal limitation improves the performance
829 of leaf and canopy models at high vapour pressure deficit, *Tree Physiol.*, 39(12), 1961–1974, doi:10.1093/treephys/tpz103,
830 2019.
- 831 Zencich, S. J., Froend, R. H., Turner, J. V. and Gailitis, V.: Influence of groundwater depth on the seasonal sources of water
832 accessed by Banksia tree species on a shallow, sandy coastal aquifer, *Oecologia*, 131(1), 8–19, doi:10.1007/s00442-001-
833 0855-7, 2002.
- 834 Zeng, X. and Decker, M.: Improving the numerical solution of soil moisture-based Richards equation for land models with a
835 deep or shallow water table, *J. Hydrometeorol.*, 10(1), 308–319, doi:10.1175/2008JHM1011.1, 2009.
- 836 Zhang, H., Pak, B., Wang, Y. P., Zhou, X., Zhang, Y. and Zhang, L.: Evaluating surface water cycle simulated by the Australian
837 Community Land Surface Model (CABLE) across Different Spatial and Temporal Domains, *J. Hydrometeorol.*, 14(4),
838 1119–1138, doi:10.1175/JHM-D-12-0123.1, 2013.
- 839 Zhou, S., Williams, A. P., Berg, A. M., Cook, B. I., Zhang, Y., Hagemann, S., Lorenz, R., Seneviratne, S. I. and Gentile, P.:
840 Land-atmosphere feedbacks exacerbate concurrent soil drought and atmospheric aridity, *Proc. Natl. Acad. Sci.*, 116(38),
841 18848–18853, doi:10.1073/pnas.1904955116, 2019.

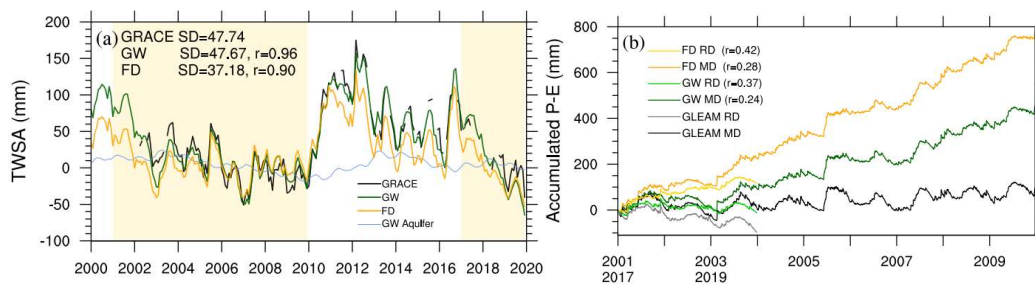


842 Zipper, S. C., Keune, J. and Kollet, S. J.: Land use change impacts on European heat and drought: remote land-atmosphere
843 feedbacks mitigated locally by shallow groundwater, *Environ. Res. Lett.*, 14(4), 044012, doi:10.1088/1748-9326/ab0db3,
844 2019.

845



846



847

848

849 **Figure 1** (a) Total water storage anomaly (TWSA) during 2000–2019 and (b) accumulated P–E for the two droughts over S.E. Australia. In
850 panel (a), observations from GRACE are shown in black, the GW simulation in green, FD in orange and the aquifer water storage anomaly in
851 GW in blue. The shading in panel (a) highlights the two drought periods. The left top corner of panel (a) displays the correlation (r) between
852 GRACE and GW/FD, as well as the standard deviation (SD, mm) of GRACE, GW and FD over the periods when GRACE and the simulations
853 coincide. Panel (b) shows the accumulated P–E for two periods; the dark lines show the 2001–2009 Millennium drought (MD) and the light
854 lines show the 2017–2019 recent drought (RD). The correlation (r) between the P and E is shown in the legend of panel (b).

855

856

857

858

859

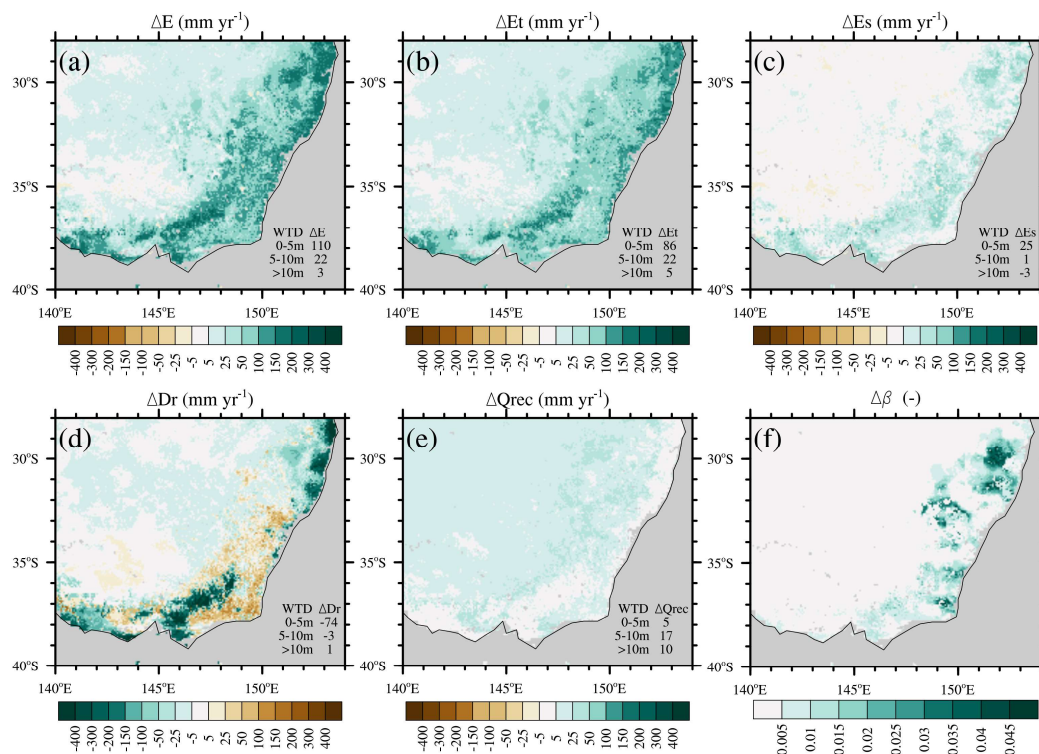
860

861

862

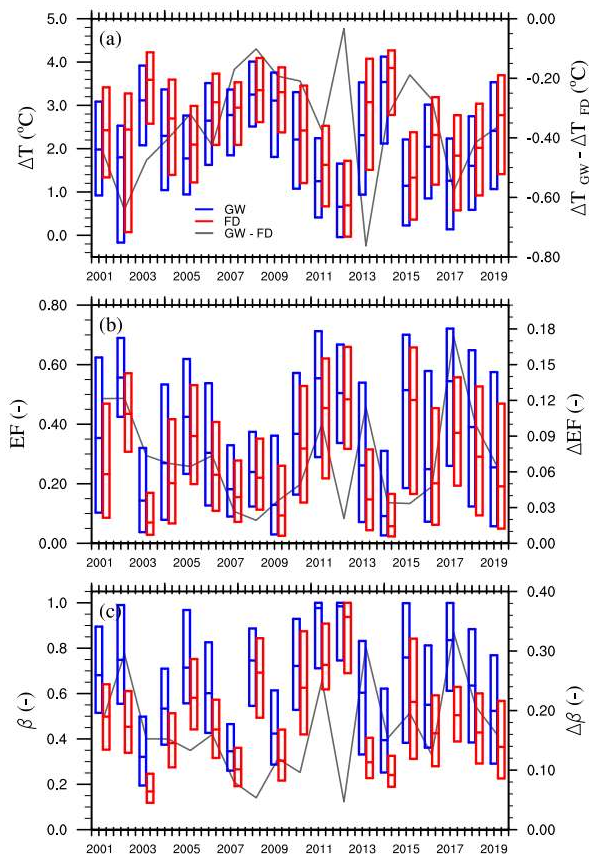
863

864



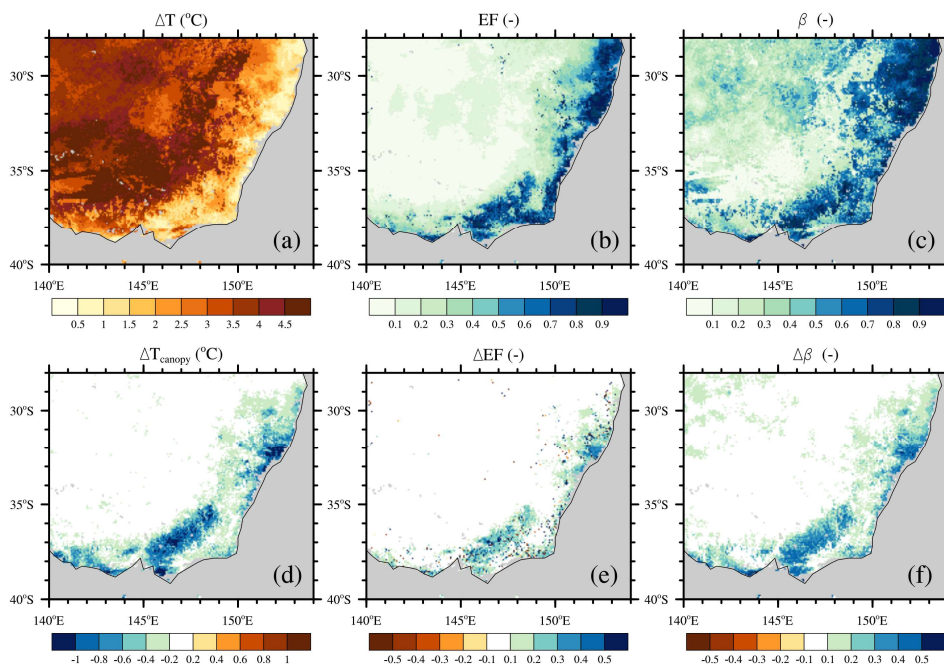
865

866 **Figure 2.** The overall influence of groundwater during the recent drought. (a)-(e) are the difference (GW-FD) in total evaporation (ΔE),
 867 transpiration (ΔEt), soil evaporation (ΔEs), vertical drainage (ΔDr) and recharge ($\Delta Qrec$), respectively. In the bottom right of panels (a)-(e),
 868 the average of each variable over selected water table depths (WTD) is provided. (f) is the maximum night-time water stress factor difference
 869 ($\Delta\beta$) between 3 am (i.e. predawn when the soil is relatively moist following capillary lift overnight) and 9 pm the previous day. We only
 870 include rainless nights in January 2019 to calculate $\Delta\beta$ to remove any influence of overnight rainfall.



871

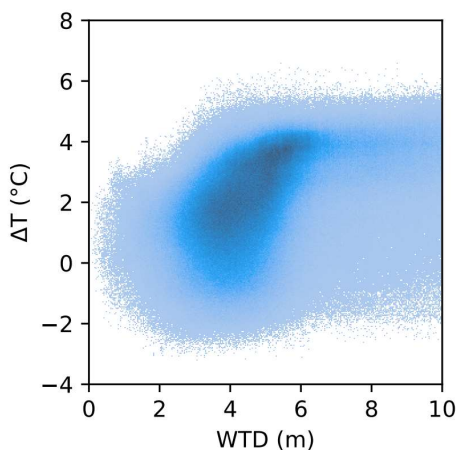
872 **Figure 3.** Groundwater-induced differences in (a) $T_{\text{canopy}} - T_{\text{air}}$ (ΔT), (b) evaporative fraction (EF) and (c) water stress factor (β) during 2000–
873 2019 summer heatwaves over forested areas. The left y-axis is the scale for boxes. The blue boxes refer to the GW experiment and the red
874 boxes to FD. For each box, the middle line is the median, the upper border is the 75th percentile, and the lower border is 25th percentile. The
875 right y-axis is the scale for the grey lines which display the difference in the medians (GW–FD).



876
 877

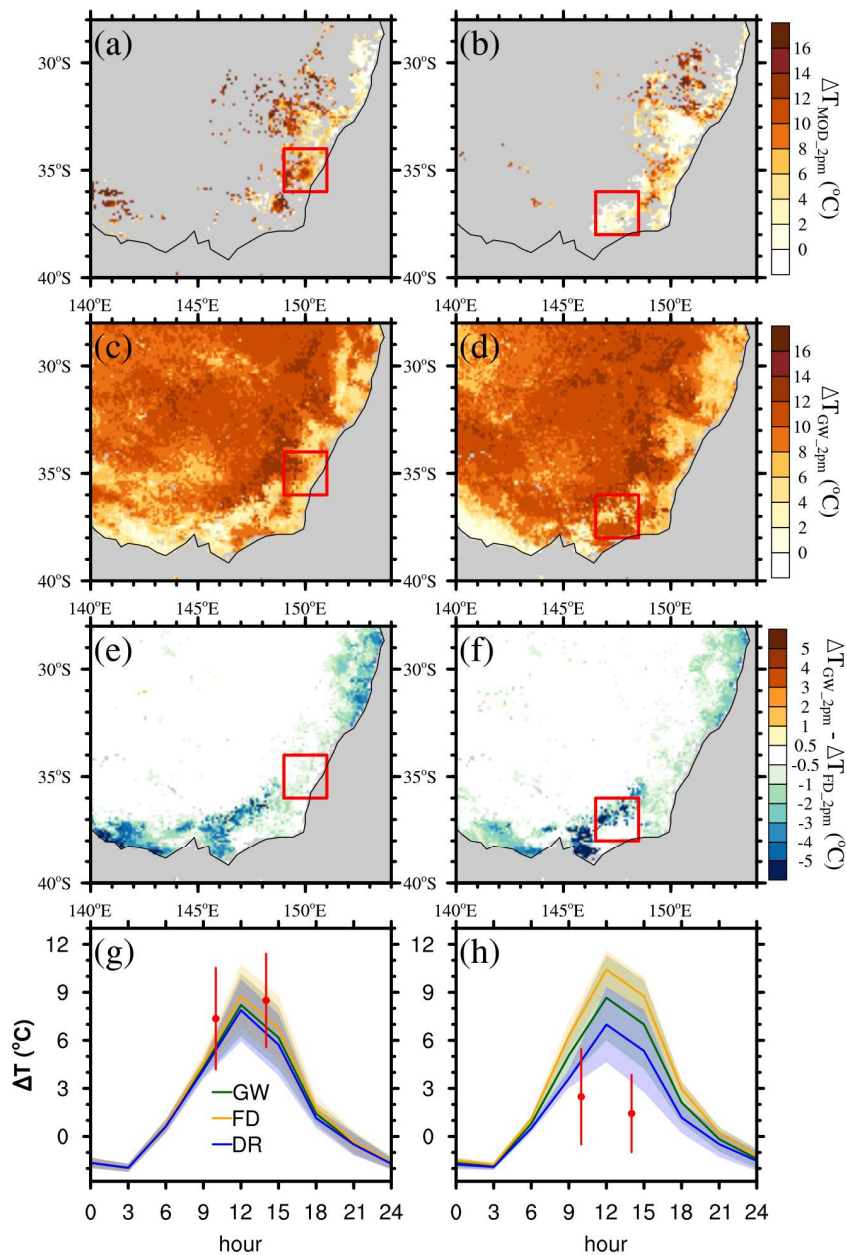
878 **Figure 4.** Land response to heatwaves during the recent drought. Panels (a)-(c) are the mean $T_{\text{canopy}}-T_{\text{air}}$ (ΔT), evaporative fraction (EF), and
 879 soil water stress factor (β) in GW, respectively, during 2017–2019 summer heatwaves. Panel (d)-(f) are the difference (GW-FD) of T_{canopy} ,
 880 EF and β . Note that the colour bar is switched between (d) and (e)-(f).

881
 882
 883



884
 885

886 **Figure 5.** A density scatter plot of $T_{\text{canopy}}-T_{\text{air}}$ (ΔT) versus water table depth (WTD) in GW simulations over forested areas in all heatwaves
 887 during 2000–2019. Every tree pixel on each heatwave day accounts for one record and the darker colours show higher recorded densities.

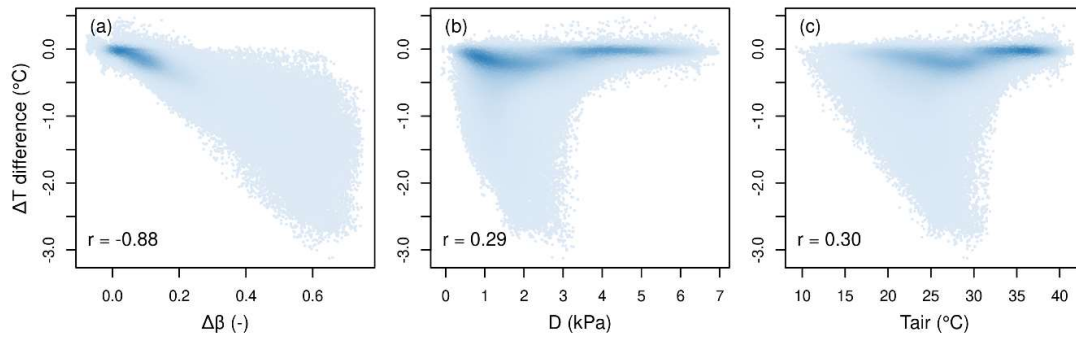


888

889 **Figure 6.** The simulation of two heatwaves on 15th (left column) and 25th January 2019 (right column). The first row shows the difference
 890 between MODIS land surface temperature (LST) and T_{air} at 2 pm (ΔT_{MOD_2pm}) (only forested areas with good LST quality data are displayed).
 891 The second row is the GW simulation of ΔT at 2 pm (ΔT_{GW_2pm}). The third row is ΔT_{GW_2pm} minus ΔT_{2pm} in FD (ΔT_{FD_2pm}). The last row is
 892 the diurnal cycle of ΔT over the selected regions shown by the red boxes in panels (e) and (f). In panel (e) and (f), the shadings show the
 893 uncertainty in every simulation defined as one standard deviation (SD) among the selected pixels. The red dots are MODIS LST minus T_{air}
 894 with the uncertainty shown by the red error bars. For both regions, only pixels available in MODIS are shown.

895

896



897

898 **Figure 7.** Density scatter plots showing the three factors that influence the difference in $T_{\text{canopy}} - T_{\text{air}}$ between GW and FD (ΔT , expressed as
899 GW–FD difference). (a) is ΔT difference against the β difference (GW–FD) ($\Delta\beta$), (b) is ΔT difference against vapour pressure deficit (D),
900 and (c) is ΔT difference against T_{air} . Each point corresponds to a tree pixel on a heatwave day in January 2019. The darker colours illustrate
901 where the records are more dense. The correlation (r) between the x- and y-axis is shown in the bottom left of each panel.

902